nature communications

Article

https://doi.org/10.1038/s41467-025-58319-y

SCFA biotherapy delays diabetes in humanized gnotobiotic mice by remodeling mucosal homeostasis and metabolome

Received: 17 April 2024

Accepted: 14 March 2025

Published online: 25 March 2025

Check for updates

Bree J. Tillett[1], Jacky Dwiyanto[2], Kate R. Secombe[1], Thomas George[1], Vivian Zhang[1], Dovile Anderson[3,4], Emily Duggan[5], Rabina Giri[6], Dorothy Loo[5], Thomas Stoll[7], Mark Morrison[1,8], Jakob Begun[6], Michelle M. Hill[7], Esteban N. Gurzov[9], Kirstine J. Bell[10], Sonia Saad[11], Christopher K. Barlow[4,12], Darren J. Creek[3,4], Chun Wie Chong[13], Eliana Mariño[12,14,15] ✉ & Emma E. Hamilton-Williams[1,15] ✉

Type 1 diabetes (T1D) is linked to an altered gut microbiota characterized by reduced short-chain fatty acid (SCFA) production. Oral delivery of a SCFA-yielding biotherapy in adults with T1D was followed by increased SCFAs, altered gut microbiota and immunoregulation, as well as delaying diabetes in pre-clinical models. Here, we show that SCFA-biotherapy in humans is accompanied by remodeling of the gut proteome and mucosal immune homeostasis. Metabolomics showed arginine, glutamate, nucleotide and tryptophan metabolism were enriched following the SCFA-biotherapy, and found metabolites that correlated with glycemic control. Fecal microbiota transfer demonstrated that the microbiota of SCFA-responders delayed diabetes progression in humanized gnotobiotic mice. The protected mice increased similar metabolite pathways to the humans including producing aryl-hydrocarbon receptor ligands and reducing inflammatory mucosal immunity and increasing IgA production in the gut. These data demonstrate that a potent SCFA immunomodulator promotes multiple beneficial pathways and supports targeting the microbiota as an approach against T1D. Trial registration: Australia New Zealand Clinical Trials Registry ACTRN12618001391268.

The gut microbiota is a key drivers of intestinal homeostasis and regulators of the developing immune system[1]. Dysbiosis of the gut microbiota has been implicated as a possible factor contributing to the development of autoimmune diseases such as type 1 diabetes (T1D)[2]. T1D is caused by a T-cell driven autoimmune attack on the insulin-producing beta cells of the pancreatic islets and is commonly diagnosed in childhood. Multiple studies have reported alterations in the gut microbiota composition preceding T1D onset, with increases in Bacteroides species, decreases in Firmicutes and decreased beta diversity all reported[3]. While the taxonomic changes observed are not always consistent between studies, a common functional deficiency has been related to T1D at various disease stages. A reduction in SCFA, acetate-, propionate- and butyrate- producing bacteria was associated with islet autoimmune responses in mice, newly diagnosed children, and in adults with longstanding T1D[4–7]. Thus, a functional defect in microbial SCFA production, rather than a deficit in specific species, may be linked to the progression of islet autoimmunity and T1D[8].

SCFAs are well known for their wide-ranging beneficial effects on the host, acting as an energy source, signaling molecules and as epigenetic regulators[9]. Butyrate is a major energy source for the colonic epithelium, improving intestinal homeostasis, stimulating mucous production, and promoting barrier function through tight-junction

A full list of affiliations appears at the end of the paper. ✉e-mail: eliana.marino@monash.edu; e.hamiltonwilliams@uq.edu.au

formation[9]. In immune cells, butyrate promotes regulatory T cell (Treg) differentiation and suppresses inflammatory cytokine production by antigen presenting cells, while acetate modulates B-cell activation and IgA production[4,7,10,11]. SCFAs also improve islet beta-cell survival in response to stress[12,13]. In addition to SCFAs, other microbially derived metabolites including arginine, tryptophan metabolites, glutamic acid, succinic acid, ornithine and citrulline have been associated with altered risk of future progression of T1D[14–17]. We hypothesize that a high-SCFA yielding intervention will remodel the gut microbiota, restoring downstream production of multiple microbial metabolites required to reprogram the progression of islet autoimmunity.

Previously, we demonstrated that a SCFA-biotherapy comprising of a polysaccharide biomolecule modified to deliver acetate and butyrate (HAMSAB) protects from diabetes development in the non-obese diabetic (NOD) mouse model of T1D[4]. The mechanism of action was due to reduced activation of islet-specific T cells, expanded Tregs and a reduction in hyperactive B cells[4]. In addition, this potent immunomodulator has been shown to have therapeutic effects in hypertension[18], which is an indicator for the effectiveness of SCFAs in treating serious or life-threatening conditions like T1D. In a recent pilot study, adults with long-standing T1D given SCFA-biotherapy for 6 weeks had increased fecal and plasma SCFAs and an altered gut microbiota[19]. This correlated with a shift in circulating immune response, characterized by decreased B-cell activation and elevated regulatory TIGIT and CTLA4 expression in T cell subsets. Though not designed to assess beta cell preservation or T1D delay, the study's findings suggest that the effects of SCFA-biotherapy on immune regulation observed in preclinical models apply to humans.

The aim of this study was to determine if SCFA-biotherapy altered mucosal immunity, gut barrier function and metabolite production, potentially reducing T1D onset. Using fecal proteomics, we showcase remodeled gut barrier proteins and innate immunity following the SCFA intervention. We identified metabolic shifts in arginine, nucleotide, and tryptophan metabolites, and then correlated these with glycemic control. We established a causal connection between SCFA-modified gut microbiota and its role in preventing or delaying T1D by transferring fecal microbiota from SCFA responder and non-responder human participants into germ-free NOD mice. We showed that the microbiota from SCFA-responders increased butyrate production and delayed diabetes progression after transfer into NOD mice, which was associated with a distinct metabolite profile, aryl hydrocarbon receptor ligand production and remodeled mucosal immunity. With broad effects on both gut barrier, immunity and metabolism, restoration of SCFA production is a promising approach for interventions designed to halt progression of T1D.

Results

Fecal human proteome remodeling following SCFA-yielding biotherapy

In NOD mice, administration of an acetate and butyrate yielding biotherapy improved gut homeostasis via increasing tight-junction and *IL22* gene expression[4]. We hypothesized that increasing SCFA delivery would also impact on mucosal immunity and gut barrier function in humans. To investigate this, we used stool samples collected from adults with long-standing T1D during a 6-week intervention of a SCFA-biotherapy, with study visits at week 0 (baseline), week 6 (end of intervention) and week 12 (follow-up), as previously described[19]. The study was a single-armed pilot trial and enrolled 21 participants, of which 18 completed the trial with stool and plasma samples used in the current study (Fig. 1A). The characteristics of the study participants are described in Supplementary Data 1.

To investigate gut barrier homeostasis in these individuals, we performed untargeted proteomic analysis of soluble stool proteins, which are enriched for human proteins derived from the gut epithelium and exocrine pancreas[20]. Searching the detected peptides against the human proteome database identified 738 human proteins after filtering. Supervised clustering using partial least-squares discriminant-analyses (PLS-DA) indicated the host fecal proteome was unique at all three timepoints and this was confirmed by PERMANOVA ($p = 0.001$), with the follow-up timepoint not returning to baseline after the intervention ceased (Fig. 1B-D). Univariate linear mixed model analysis found 159 proteins that differed between the timepoints ($p < 0.05$), with 53 of these having a false discovery rate (FDR) < 0.05 (Supplementary Data 2, Supplementary Fig. 2).

Gene Ontology pathway enrichment analysis of proteins that increased following SCFA-biotherapy found 201 enriched biological processes at 6 weeks (FDR < 0.05, Fig. 1E, Supplementary Data 3). The most enriched process was cell redox homeostasis, which included antioxidants peroxiredoxin-6 (PRDX6), thioredoxin (TXN), and thioredoxin reductase 1 (TXNRD1), which protect from oxidative stress[21]. Concordant with this, proteins associated with response to hypoxia and response to decreased oxygen levels were enriched, suggesting a lower oxygen environment. Actin filament pathways, fiber organization, and epithelial cell differentiation were increased, driven by epithelial-cell junction proteins CAPZB, CAPZA1, and radixin (RDX). Multiple innate immune processes were enriched related to neutrophils and myeloid cells including anti-inflammatory protease progranulin (GRN), anti-microbial defense protein NOX2 and proteins involved in cell adhesion, migration and angiogenesis such as grancalcin (GCA), integrin subunit alpha M (ITGAM or CD11b), and matrix metallopeptidase-9 (MMP9) (Supplementary Fig. 1, Supplementary Data 3). At follow-up, epithelial and neutrophil and myeloid cell pathways remained enriched demonstrating persistent effects after the end of the intervention (Supplementary Data 3).

Pathway enrichment using KEGG found 19 pathways were significantly enriched at 6 weeks (FDR < 0.05, Fig. 1F, Supplementary Data 4). These included innate immune pathways, indicating a strong involvement of neutrophils and phagosomes. Tight junction pathways driven by TUB1A, RDX, and SLC9A3R1 increased (Supplementary Fig. 1), as were protein processing in the endoplasmic reticulum including heat shock proteins involved in suppressing aggregation of mis-folded proteins (CRYAB, HSP90B1, and PRKCSH). Enrichment of alanine, aspartate, and glutamate metabolism and arginine biosynthesis included arginosuccinate synthase-1 (ASS1), CAD protein (CAD) and 4-aminobutyrate aminotransferase (ABAT), nitric oxide synthase (NOS2) and aldehyde dehydrogenase 2 (ALDH2), which all increased after SCFA-biotherapy (Supplementary Fig. 1). At follow-up, lysosome and phagosome pathways were enriched suggesting durable innate immune responses (Supplementary Data 4).

KEGG pathways that decreased after SCFA biotherapy included ferroptosis and necroptosis cell death pathways (Fig. 1G, Supplementary Data 4). These were driven by iron storage proteins, ferritin light chain and ferritin heavy chain 1, and the voltage-dependent anion-selective channel protein, a prop-apoptotic protein (Supplementary Fig. 1). Necroptosis is an inflammatory form of cell death often resulting from pathogen-induced cell damage[22]. Ferroptosis is an iron-associated form of cell death linked to a failure of antioxidant defenses and is associated with dysfunction of the intestinal epithelium and gut disease[22]. Similar pathways persisted at follow-up with necroptosis remaining downregulated (Supplementary Data 4). Together, these data suggest that a neutrophil-mediated tissue-repair process may be activated following SCFA biotherapy, accompanied by an increase in tight junction proteins and a reduction in cell-death pathways.

Metabolite production in the gut is significantly altered following SCFA biotherapy

As metabolites produced by the gut microbiota are likely mediators of any effects of SCFA biotherapy on the gut epithelium, we used untargeted metabolomics to broadly profile fecal metabolites, including

https://doi.org/10.1038/s41467-025-58319-y

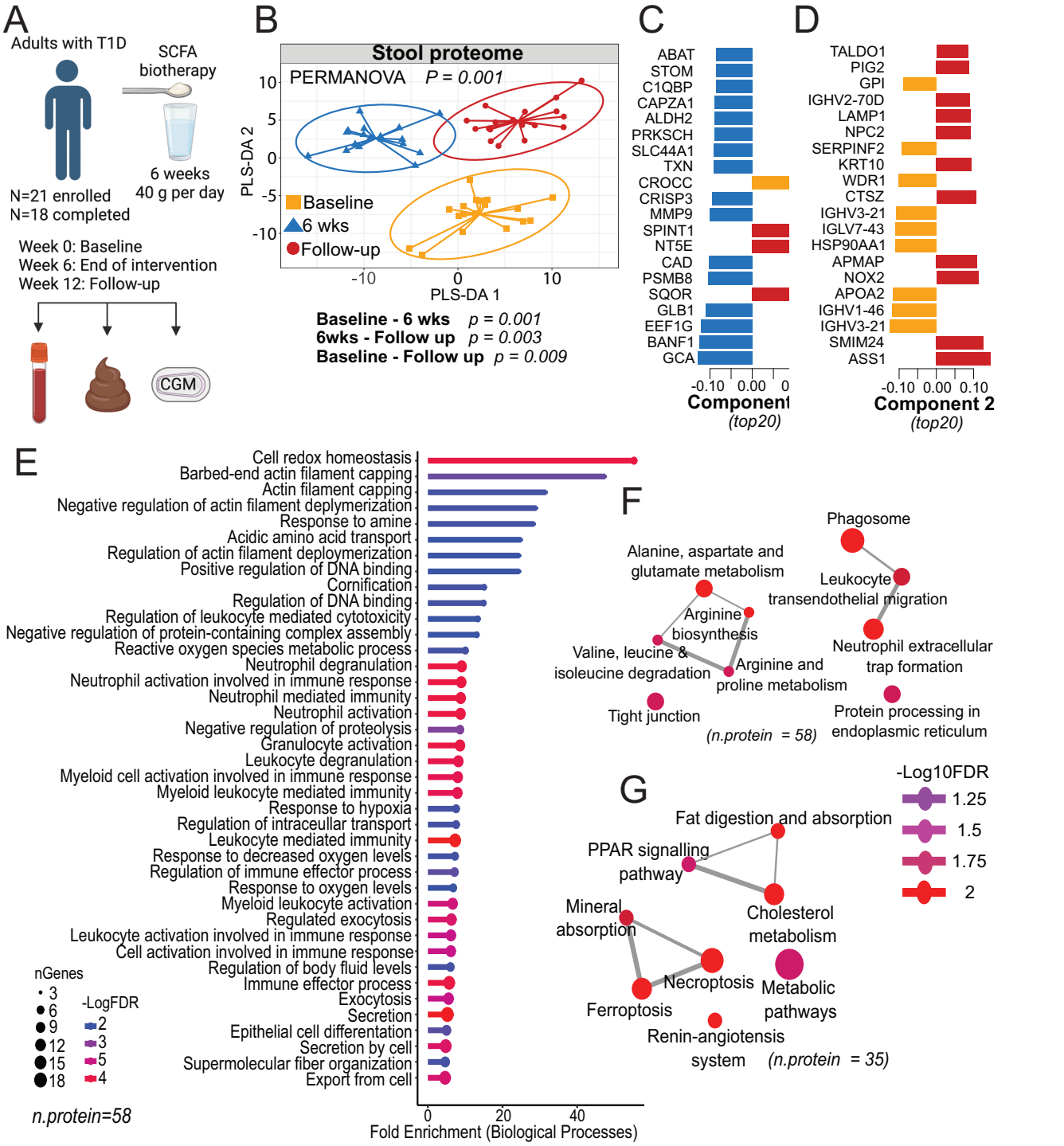

Fig. 1 | Gut barrier protein remodeling revealed through fecal proteomics after SCFA biotherapy. A Schematic overview of the trial. Created in BioRender. Hamilton-Williams, E. (2025) https://BioRender.com/h13m098. **B** Multivariate PLS-DA of human stool proteins. Significance determined by two-sided PERMANOVA. Pairwise comparisons were adjusted for multiple correction by false discovery rate. Ellipses show the 95% confidence interval. **C**, **D** PLS-DA components 1 and 2, top 20 loadings. Orange: baseline, blue: week 6, red: follow-up. **E** Top-40 significantly enriched Gene Ontology biological processes (FDR < 0.05) enriched using proteins ($p < 0.05$) that increased from baseline to 6 weeks. **F** KEGG pathway enrichment of proteins which increased from baseline to six weeks or **G** decreased from baseline to six weeks. Significance determined by linear mixed effects models using a Likelihood Ratio Test ($p < 0.05$) and Benjamini-Hochberg correction for multiple testing. Enrichments were performed using proteins with $p < 0.05$. The cut-off for edges is 40% shared proteins. Thickness of edges indicate degree of protein overlap. See also Supplementary Fig. 1 and Supplementary Data 2-4.

metabolites produced by the microbiota and the host. LC/MS analysis detected 603 putatively annotated metabolites. Supervised multivariate analysis showed that the fecal metabolome at 6 weeks was distinct from the other two timepoints (PERMANOVA $p = 0.006$, Fig. 2A, Supplementary Fig. 2A). Univariate analysis found 101 metabolites with $p < 0.05$, of which eight had an FDR < 0.05 (Fig. 2B, Supplementary Fig. 2B, Supplementary Data 5). MetOrigin pathway analysis identified an enrichment of multiple pathways including

https://doi.org/10.1038/s41467-025-58319-y

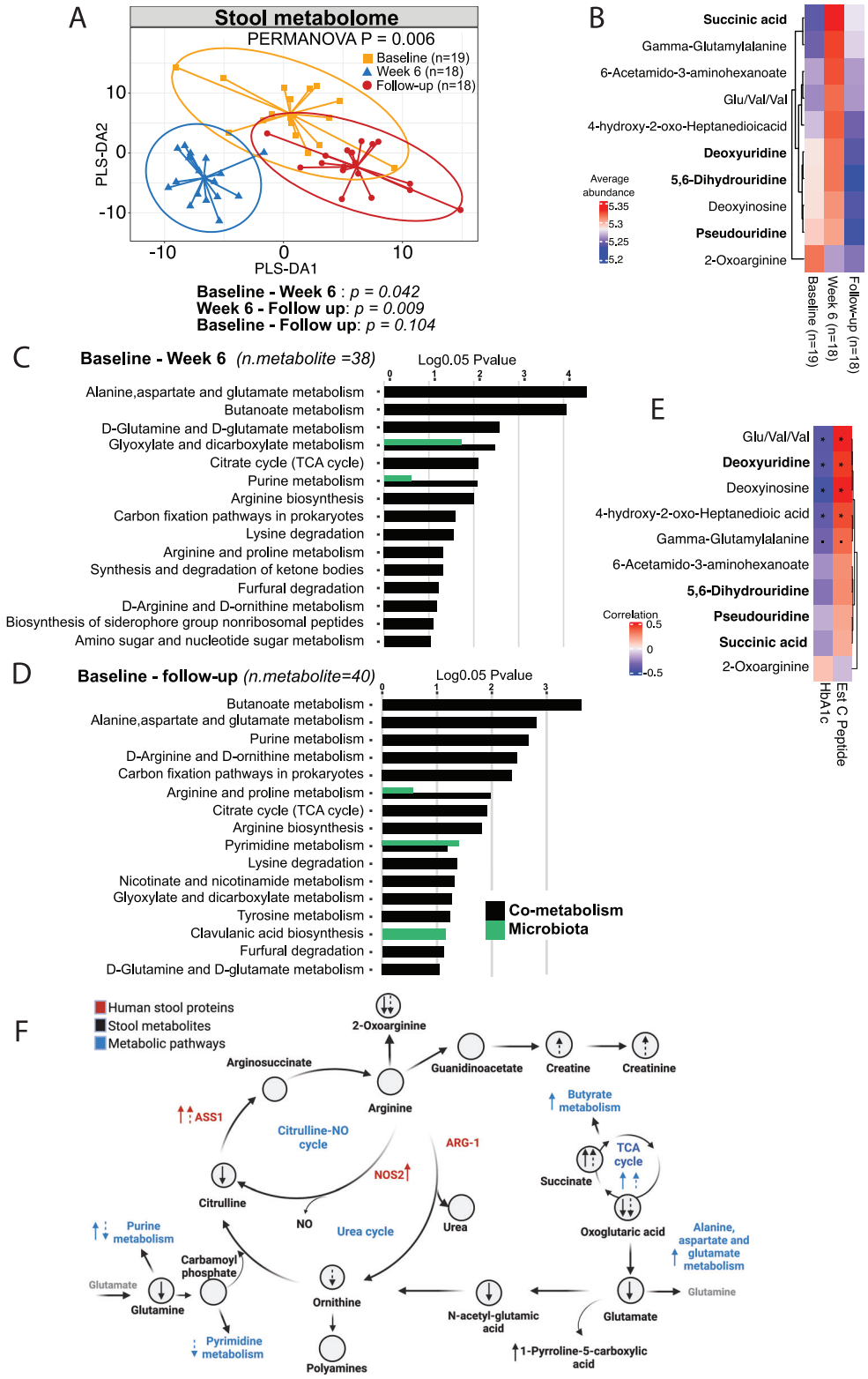

alanine, aspartate and glutamate metabolism, butanoate metabolism, arginine biosynthesis, TCA cycle, and purine metabolism at both 6 weeks and follow-up, with the majority of pathways shared by both host and microbiota (Fig. 2C, D, Supplementary Data 6). Pyrimidine metabolism, driven in part by microbiota-specific pathways, was enriched at follow-up (Fig. 2C, D, Supplementary Data 6). Within these pathways, increases in succinic acid (succinate) and butyric acid (butyrate) at both 6 and 12 weeks contributed to the butanoate pathway enrichment (Supplementary Fig. 2C). Butyrate is a major source of energy for colonocytes through the TCA cycle (which includes succinate)[23]. Arginine pathway enrichment was driven by increased 1-pyrroline-5-carboxylic acid at 6 weeks and increased creatine at 12 weeks and decreases in ornithine, glutamine, and 2-oxoarginine Supplementary Fig. 2C, Supplementary Data 6). Alanine, aspartate, and

Fig. 2 | Gut metabolite production undergoes significant changes after SCFA biotherapy. A Multivariate PLS-DA of human stool metabolites. Significance determined by two-sided PERMANOVA. Pairwise comparisons were adjusted for multiple corrections by false discovery rate. Ellipses show a 95% confidence interval. **B** Abundance heatmap of stool metabolites with an FDR < 0.1 determined by linear mixed effects model using a Likelihood Ratio Test ($p < 0.05$) and Benjamini-Hochberg correction for multiple testing. Metabolites in bold are level 1 (identified using reference standards). **C** Significant KEGG pathways enriched from baseline to six weeks and **D** baseline to follow-up. Enrichments were performed in MetOrigin using metabolites with $p < 0.05$. Differences were determined using paired two-tailed t-test of individual metabolites with a cut-off value of $p < 0.05$. Green bars: microbiota pathways, black bars shared host and microbiota (co-metabolism) pathways. **E** Repeated measures correlations of metabolites with FDR < 0.1 with glycemic variables. * indicates FDR corrected p-value > 0.01 < 0.05 and · indicates p-value > 0.05 < 0.1 **F** Pathway schematic showing key human stool proteins, stool metabolites, and metabolic pathways altered after the intervention. Solid arrow indicates changes at 6-weeks, dashes arrow indicates changes at follow-up. TCA cycle: The citric acid cycle, NO: nitric oxide. Created in BioRender. Hamilton-Williams, E. (2025) https://BioRender.com/l00t262. See also Supplementary Fig. 2 and Supplementary Data 2, 5, and 6.

glutamate pathway enrichment was driven by decreases in alanine, oxoglutaric acid, and glutamine, but increased succinic acid (Supplementary Fig. 2C, Supplementary Data 6). Purine and pyrimidine nucleotide metabolism pathways included deoxyinosine, deoxyuridine, and pseudouridine, which all tended to increase at 6 weeks, and significantly dropped at 12 weeks (Supplementary Fig. 2B, C, Supplementary Data 6). Deoxyinosine and deoxyuridine, along with a tripeptide containing a glutamic acid and two valines (Glu/Val/Val), 4-hydroxy-2-oxo-heptanedoic acid, and gamma-glutamylalanine negatively correlated with HbA1c and positively correlated with estimated C-peptide (Fig. 2E).

A combined analysis of the stool metabolites, pathways and stool proteins supports the hypothesis that the SCFA biotherapy is driving the TCA cycle and alanine, aspartate, and glutamate metabolism leading to glutamate and glutamine being converted into purine and pyrimidine nucleotides, as well as driving the urea cycle and arginine metabolism (pathway schematic shown in Fig. 2F). Most changes from baseline to 6 weeks were precursor metabolites involved in arginine biosynthesis such as the stool metabolites N-acetyl-glutamic acid, glutamine and glutamate. Whereas changes from baseline to follow-up were metabolites involved in arginine utilization such as the stool metabolites creatine, creatinine and 2-oxoarginine (Fig. 2F).

Plasma metabolomics reveals systemic metabolic effects following SCFA-biotherapy

To further understand how the 6-week SCFA-biotherapy in adults with T1D, and the associated changes in the microbiome and metabolome influenced the host systemically, we investigated circulating metabolites in plasma. Untargeted LC/MS analysis of plasma identified 619 putatively annotated metabolites. Multivariate PLS-DA showed the greatest effect on plasma metabolites at follow-up, and this was significant by PERMANOVA ($p = 0.022$, Fig. 3A, B). Univariate analysis found 92 metabolites had a $p < 0.05$ using a linear mixed model (Supplementary Data 7). Succinic acid was increased at follow-up compared with 6 weeks and 2-oxoarginine decreased at week 12, similar to the stool metabolome (Supplementary Data 7). An exploratory enrichment analysis found tryptophan metabolism and phenylalanine, tyrosine and tryptophan biosynthesis were the most impacted pathways at 12 weeks (Fig. 3C, Supplementary Data 8), which was attributed to tryptophan, kynurenine, and indolepyruvate (Supplementary Data 8). Valine, leucine, and isoleucine biosynthesis and degradation were also enriched. These data suggest that there is a sustained systemic impact on metabolic pathways following SCFA biotherapy.

Human to mouse microbiota transfer model demonstrates disease-modifying effects of the SCFA-biotherapy modified microbiota

We next used a human-to-mouse fecal microbiota transfer model to investigate whether the functional changes in the human microbiota present after the SCFA-biotherapy could modify disease progression (Fig. 4A). Given HAMSAB significantly increased the concentrations of acetate, butyrate and propionate in feces and circulation in both mice[4] and humans[19], we classified participants from the trial based on their increase in stool SCFAs at 6-weeks, with a fold change ≥2 termed 'responders' and <2 as "non-responders" (Fig. 4B). We selected $n = 2$ SCFA non-responders (donors A and B) and $n = 2$ responders (donors C and D) that also had a high live bacteria count. While responder and non-responder subjects similarly altered their alpha and beta diversity following the biotherapy Supplementary Fig. 3, the responder individuals tended to have higher alpha diversity. Resuspensions of individual human donor stool samples were gavaged into female germ-free NOD mice prior to mating and the female offspring was studied for microbiota colonization, metabolite levels, and diabetes progression (Fig. 4A). A control group of dams was gavaged with sterile saline (PBS) and their offspring remained germ-free.

All of the mice remained on a standard diet throughout the experiment. Interestingly, fecal butyrate in the offspring was the only SCFA significantly higher from the mice colonized from the post-intervention responder samples (6-week donor samples, $p = 0.0282$) compared to the non-responder colonized mice and higher than both groups colonized with the baseline donor samples (Fig. 4C, Supplementary Fig. 4, $p = 0.0061$).

The mice colonized with the post-SCFA-biotherapy microbiota from responders at 6 weeks showed a notable delay in diabetes progression compared to both the non-responder group at the same time point ($p = 0.0198$) and the PBS control germ-free group ($p = 0.0087$) (Fig. 4D). In contrast, mice colonized with the baseline samples from either the responders or non-responders failed to significantly delay diabetes in colonized mice compared to the PBS control group (Fig. 4E). A second cohort of germ-free female NOD mice were similarly colonized and analyzed at 10-weeks of age for their immune cell and pancreas phenotype. Histology and immunofluorescence staining trended to reduced mononuclear cell infiltration and insulin content in islets from the responder compared to the non-responder colonized mice (Fig. 4F, Supplementary Fig. 5). A lower proportion of BDC2.5 islet-specific $CD4^+$ T cells identified by tetramer staining were found in the pancreatic lymph nodes of the responder mice colonized with the post-biotherapy microbiota ($p = 0.0448$, Supplementary Fig. 6). Additionally, the responder mice had increased $Foxp3^+CD8^+$ regulatory T cells in the spleen ($p = 0.053$) and pancreatic lymph nodes ($p = 0.0099$). The data suggest that the microbial changes caused by SCFA intervention in humans still impact the development of autoimmunity in mice after adoptive transfer, with the protective effects primarily associated with butyrate response.

Diabetes-protected responder colonized mice cluster by fecal metabolites, not microbiota composition

Colonization of the fecal microbiota in both the gavaged mothers and the female offspring was investigated using 16S rRNA sequencing. Similar to previous studies[24], alpha diversity in the colonized mice samples was lower than in the human donor samples (Supplementary Fig. 7). However, multivariate PLS-DA showed that the human donor samples clustered with their respective colonized mouse samples (Supplementary Fig. 7). While there were differences in abundance of taxa between the donor human samples and the mice, there was

https://doi.org/10.1038/s41467-025-58319-y

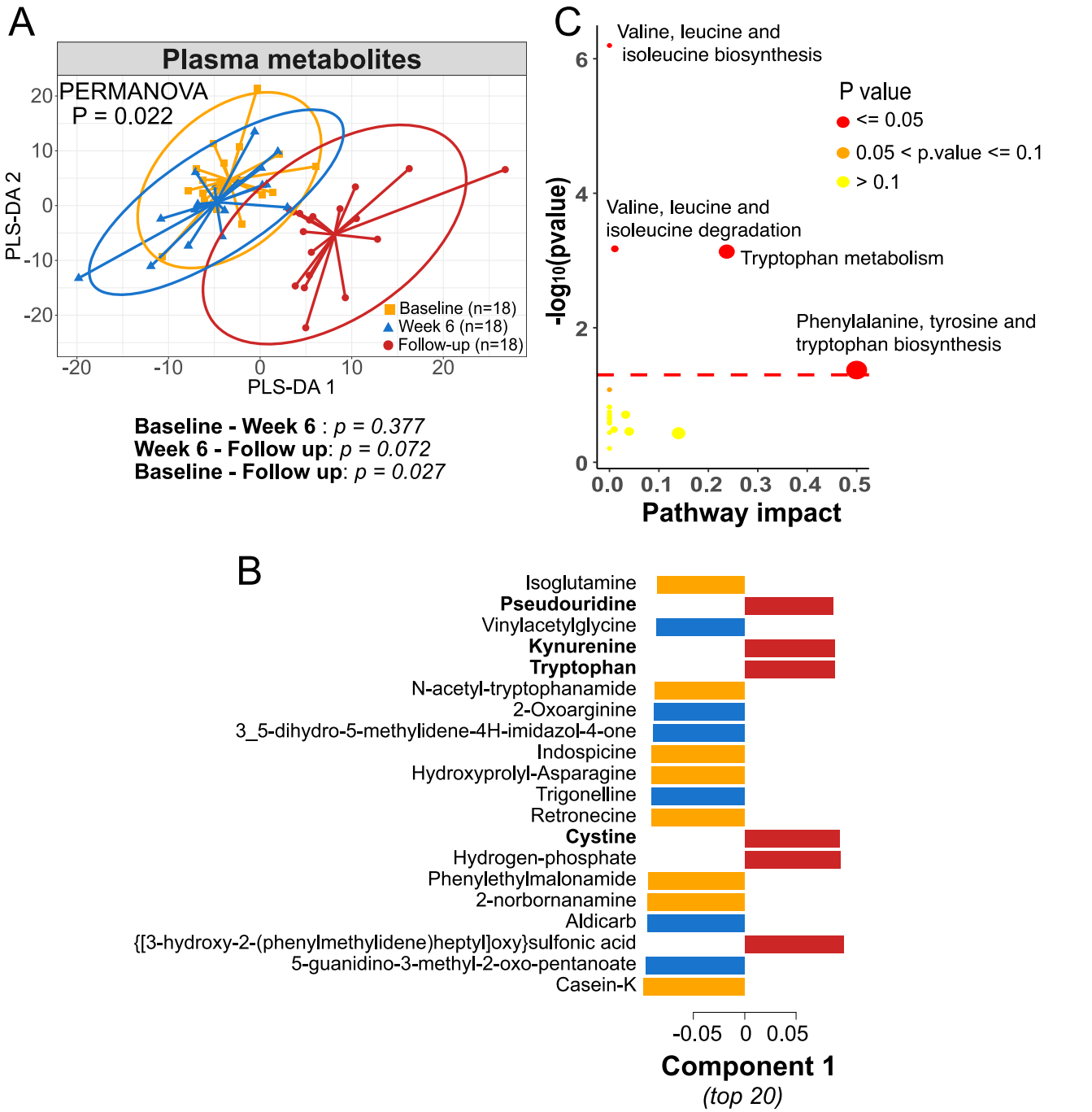

Fig. 3 | Plasma metabolites are significantly altered at follow-up. A PLS-DA analysis of plasma metabolites and **B** loading plot for component 1 of the PLS-DA. Significance determined by two-sided PERMANOVA. Pairwise comparisons were adjusted for multiple correction by false discovery rate. Ellipses indicate 95% confidence intervals. Orange: baseline, blue: week 6, red: follow-up. Metabolites in bold are level 1 (identified using reference standards). **C** MetaboAnalyst pathway enrichment analysis of plasma metabolites that changed from 6-weeks to follow-up and baseline to follow-up. Enrichment used metabolites with two-sided linear mixed model analysis $p < 0.05$. Red dashed line indicates pathway significance. Color represents the significance. Dot size represents impact. *P* values are provided. See also Supplementary Data 7 and 8.

colonization with 50.1% ± 3.6% (mean ± SD) of donor-derived species into the dams. High transmission occurred from the mothers to the offspring (mean 44.1% ± 8.3% of donor species present at 5 weeks of age), and colonization was relatively stable across time (mean 44.8% ± 9.9% of donor species present at 11 weeks of age), (Supplementary Fig. 8). Unsupervised PCA multivariate analysis demonstrated that the microbiota composition of the mice colonized from each of the four donors was distinct (Fig. 5A, Supplementary Fig. 9A, B, PERMANOVA $p < 0.001$). While there was clustering by timepoint (baseline or 6-week donor samples), the donor effect was dominant, with 83 taxa significantly differing between the four donors (FDR < 0.05, Supplementary Data 9). Notably, the "responder" and "non-responder" donors did not cluster together, with donor D more dissimilar than the other three groups. We still found that 42 taxa significantly differed between the responder and non-responder groups with genera including *Parasutterella*, *Lachnospiraceae*, *Alistipes*, and *Blautia* higher in responders while *Enterococcus*, *Turicibacter*, and *Butyricimonas* were higher in non-responder colonized mice (Supplementary Data 10).

https://doi.org/10.1038/s41467-025-58319-y

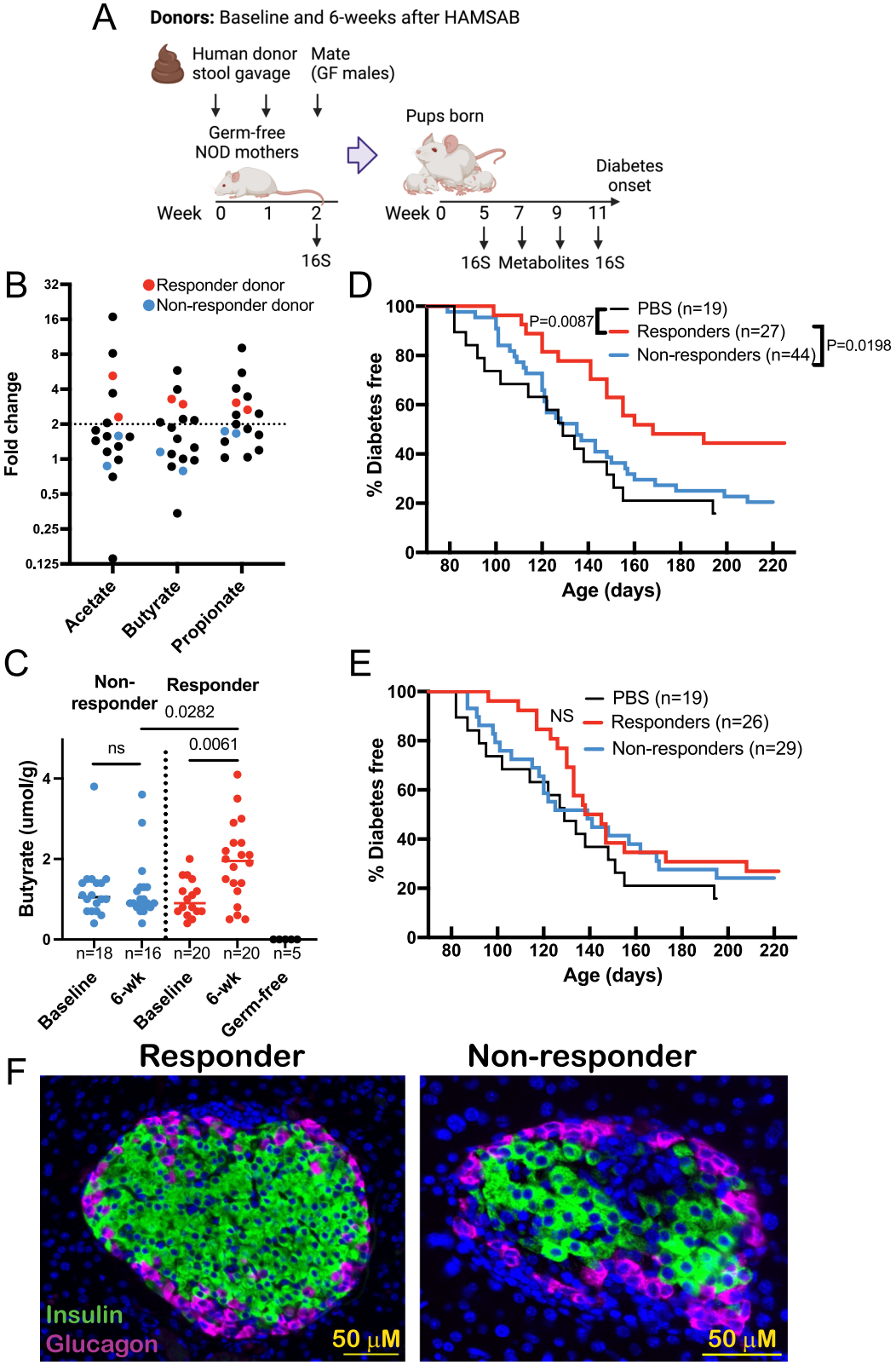

We next profiled the fecal metabolome of the colonized offspring (6-week sample colonized groups only), identifying 527 metabolites after filtering. In contrast to the microbiota composition, PCA multivariate analysis showed that the two responder groups had a similar metabolite profile distinct to the non-responders (Fig. 5B, Supplementary Fig. 9C). PERMANOVA analysis confirmed that the metabolites significantly differed between the donors ($p < 0.001$), with 302 individual metabolites differing between the responders and non-responders (FDR < 0.05, Supplementary Data 11). Pathway enrichment found that purine, pyrimidine, arginine, and glutamate metabolism were the most enriched pathways in the responder compared to the non-responder group (Fig. 5C, Supplementary Data 12). Multiple purines and pyrimidine pathway constituents were higher in responders, as were arginine precursor metabolites glutamate and oxoglutaric

Fig. 4 | Human-to-mouse microbiota transplantation from responders delays diabetes in NOD mice. A Experimental design. Female germ-free NOD mice were colonized with a human stool suspension or remained uncolonized (PBS controls) by oral gavage on days 0 and 7, then mated one week later. Female offspring were followed for diabetes progression and fecal samples collected for analysis. Created in BioRender. Hamilton-Williams, E. (2025) https://BioRender.com/u03r698. **B** Donor samples, represented by blue dots (non-responder donors) and red dots (responder donors), from four participants were selected from the $n = 18$ completed SCFA biotherapy trial participants based on fold-change in fecal butyrate at 6 weeks from baseline. One outlier individual is excluded from the graph with fold-changes of 73.2, 123.8, and 299.5. The dashed line represents fold-change of 2 cut-off for defining responder status. **C** Fecal butyrate in the female offspring of the mice (7–9 weeks of age) colonized with responder (red) or non-responder (blue) human donor stool samples (baseline and 6-week trial timepoints), or control germ-free mice. The line represents median value. Significance based on one-way ANOVA with Tukey's correction. Survival curve analysis (log-rank Mantel-Cox) test in germ-free NOD mice colonized with non-responder vs responder stool samples collected from donors at 6-weeks (**D**) or baseline (**E**) or control germ-free mice which received a sterile PBS gavage. Diabetes data was pooled from two independent experiments. **F** Pancreas sections stained by immunofluorescence for insulin (green) and glucagon (magenta), with DAPI nuclear stain (blue) from female colonized mice at 10 weeks of age ($n = 7$ responder and $n = 9$ non-responder mice, from one experiment). Representative image is shown at 20× magnification. See also Supplementary Fig. 3–6.

acid, while arginine itself and ornithine were lower (Fig. 5D, E). In addition, tryptophan metabolism was altered in the responder mice (Fig. 5D), driven by a highly significant elevation of quinic acid, a microbiota-only pathway metabolite, in responder mice (FDR = 2.18E-08). These metabolite changes and pathways enriched in the responder group showed a high similarity to the enriched pathways observed after SCFA biotherapy in the human trial participants (Fig. 2C, D).

Responder colonized mice have reduced mucosal B cell gene networks

We next investigated mucosal immunity and the gut barrier in the mice colonized with the responder versus non-responder donor microbiota via transcriptomics. At 10 weeks of age, colon and ileum tissue was collected and used for RNA sequencing from mice that had been colonized with either responder (donor C) or non-responder (donor B) 6-week sample microbiota. There were 143 differentially expressed genes in the ileum and 16 in the colon (Fig. 6A, Supplementary Data 13). Gene ontology analysis found multiple pathways related to B-cell activation and immunoglobulin production, innate immune responses, inflammatory response, defense response to bacteria and response to lipopolysaccharide were enriched in the non-responder ileum tissue (Fig. 6B, Supplementary Data 14). The strong enrichment for B-cell pathways in non-responders included *Ighg1*, *Ighg3* and *Ighd* antibody heavy-chain genes, but not IgA heavy-chain, as well as genes related to B-cell activation such as *Cd40*, suggesting that the type of antibodies secreted into the mucous layer and the lumen switches between responder and non-responder mice. KEGG enrichment identified several genes involved in tryptophan metabolism that were downregulated in responder mice including *Cyp1a1, Kmo*, and *HAAO* (Fig. 6C). *Cyp1a1* is a negative regulator of tryptophan metabolite signaling via the aryl hydrocarbon receptor (Ahr), acting to degrade Ahr ligands[25]. KEGG enrichment also found NFκB signaling and cytokine receptor interactions as well as B cell receptor signaling were downregulated in responder mice (Fig. 6C and Supplementary Data 15). These data suggest that inflammatory mucosal immunity, in particular antibody production, is reduced by colonization with the microbiota-derived from SCFA-biotherapy responder donors.

To further investigate the activation status of immune cells in the mice, we analyzed antigen-presenting cell phenotypes in a group of 10-week offspring. Consistent with the gene expression data, we found that CD40 expression on IgM^- B cells was higher in the mice colonized with 6-week sample microbiota from non-responders. In parallel to this, total conventional dendritic cells and type-2 dendritic cells had higher CD40 expression in the non-responder colonized mice. This suggests that both class-switched IgM^- B-cells and dendritic cells are more activated in the non-responder colonized mice.

Responder colonized mice have increased aryl hydrocarbon receptor ligand production

As the metabolism of tryptophan into Ahr ligands is a key mediator of intestinal homeostasis by the gut microbiota, we investigated Ahr ligand activity within the responder colonized mice. We stimulated Ahr-luciferase reporter cells with fecal water isolated from the fecal pellets of the colonized mice (Fig. 7A). We found that the fecal water of the responder mice had higher Ahr stimulatory activity than the non-responder mice, both in the baseline ($p < 0.0001$) and 6-week sample ($p < 0.0001$) colonized mice. Ahr stimulation activity increased in the 6-week sample colonized mice of both groups. We then used fecal waters from the human study participants and confirmed that Ahr ligand activity significantly increased at 6-weeks after the intervention ($p = 0.0029$, Fig. 7B). Of note, the two responder donors had higher Ahr activity than the non-responder donors at all three timepoints. Using immunofluorescence staining, we found that Ahr and IgA protein were both higher in the ileum tissue of the responder mice compared with the non-responder mice (Fig. 7C). This suggests that increased Ahr ligand availability after the SCFA-biotherapy is associated with diabetes protection.

To identify specific metabolites that may underlie the differences in Ahr activity, we re-interrogated our metabolomic datasets using an "in silico" targeted analysis of key tryptophan pathway metabolites (Supplementary Fig. 10). This analysis identified xanthurenic acid, a tryptophan metabolite with known Ahr stimulating activity downstream of kynurenine[26], was significantly higher in the mice colonized with the 6-week responder donor microbiota ($p = 0.0013$, Supplementary Fig. 10A). In the human stool metabolome, 2,8,dihydroxyquinoline and xanthurenic acid increased at 6 weeks and decreased at follow-up. Xanthurenic acid tended to be higher in the responder individuals at 6 weeks (Supplementary Fig. 10B). In the serum, tryptophan metabolites including tryptophan, kynurenine, and xanthurenic acid were all elevated at follow-up (Supplementary Fig. 10C). These data suggest that xanthurenic acid may be a key Ahr activating metabolite in both the mouse and human study.

Multi-omic factor analysis correlates microbiome markers, metabolites, stool proteins, and aryl hydrocarbon receptor ligand production with glycemic control measures

We next used multi-omic factor analysis (MOFA) to understand the relationships between the different datasets in our human study (stool proteome and metabolome, plasma metabolome and stool metagenome, microbial taxa and pathways), clinical measures, SCFA and Ahr. The MOFA approach identifies latent factors comprising correlated variables selected from the different datasets in the model, which explain the underlying variation in the data (Supplementary Data 16)[27]. We then correlated these latent factors with clinical measures of glycemic control, SCFAs and Ahr activity. The MOFA model identified 6 latent factors, with all five datasets contributing (Supplementary Fig. 11A). Latent factor 3 positively correlated with all three stool SCFAs and estimated C-peptide (Fig. 8A). Latent factor 3 positive variables were mainly plasma metabolites, including the tryptophan metabolites indolelactic acid, kynurenine, tryptophan and indolepyruvate (Fig. 8B). Variables that negatively contributed to latent factor 3 included many stool metabolites such as pseudouridine, xanthine, oxoglutaric acid,

https://doi.org/10.1038/s41467-025-58319-y

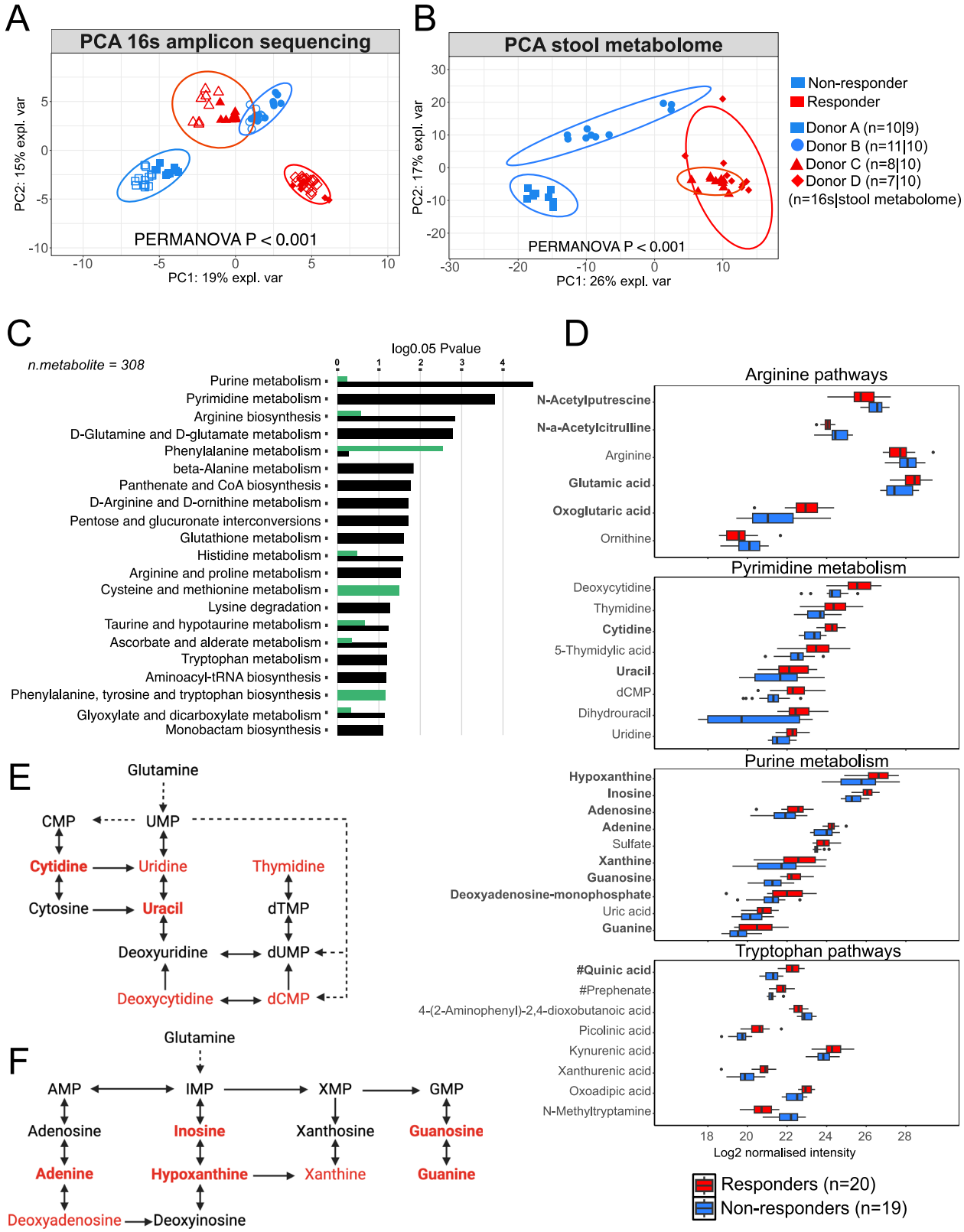

and ornithine, which decreased after the biotherapy. Latent factor 4 positively correlated with stool and plasma butyrate and Ahr activity, while negatively correlated with HbA1c (%) and basal insulin (%). Latent factor 4 was driven by *Bifidobacterium adolescentis* and microbial pathways that increased at 6 weeks such as TCA cycle, glycolysis pathways and homolactic fermentation (Supplementary Fig. 11B)[19]. Latent factor 1 negatively correlated with stool Ahr activity and plasma acetate and was driven in the negative direction by taxa (*Parabacteroides distasonis* and *Bacteriodes uniformis*) and metagenomic pathways related to pyrimidine and purine metabolism (Supplementary Fig. 11C), variables which increased at 6-weeks. Latent factor 2 was negatively contributed to by similar taxa and also negatively correlated with Ahr activity, HbA1c and basal insulin % (Supplementary Fig. 11D). Together, this integrative analysis supports that SCFA, plasma

Fig. 5 | Fecal metabolites, not gut microbiota composition, drive clustering of recipient mice in human-to-mouse microbiota transplantation study. A Sparse-PCA of 16S rRNA amplicon sequencing of feces collected from female NOD offspring of human-microbiota colonized mice at 5 weeks of age. Mice colonized with 6-week donor samples were shown. **B** PCA of fecal metabolites from female NOD mice pups collected at 7–9 weeks of age. Mice colonized with 6-week donor samples only were analyzed for metabolites. Significance determined by two-sided PERMANOVA. **C** Pathway enrichment analysis of metabolites from mice colonized with responder versus non-responder donors using MetOrigin. Differences were determined using a paired two-sided t-test of individual metabolites with a cut-off value of $p < 0.05$. Green bars− microbiome pathways, black bars−co-metabolism (shared between host and microbiota) pathways. **D** Abundance (log2 normalized intensity) of key metabolites from pathways identified in the enrichment analysis. Metabolites marked with # are microbiota only pathways determined from the origin-based MPEA analyses. 4-(2-Amino-3-hydroxyphenyl)-2,4-dioxobutanoic acid is the complete name for abbreviated metabolite in the tryptophan pathways. Box and whisker plots show median and inter-quartile range, with lines representing the minimum and maximum values. Schematic of **E** purine metabolism pathway and **F** pyrimidine metabolism pathway. Metabolites in bold are level 1 (identified using reference standards). Metabolites shown in red were higher in responder mice. Schematics created in BioRender. Hamilton-Williams, E. (2025) https://BioRender.com/w72e215 and https://BioRender.com/s39p554. See also Supplementary Fig. 7–9 and Supplementary Data 9–12.

tryptophan metabolites, and stool Ahr activity are all associated with clinical features of glycemic control in T1D.

Discussion

This is the first study to demonstrate remodeling of mucosal immunity and the gut barrier response after delivery of a potent SCFA-yielding intervention in adults with T1D. We demonstrated an increase in gut-derived antioxidant proteins, neutrophil repair and innate immune responses, epithelial and tight junction proteins, and amino acid metabolism along with a decrease in cell death pathways after delivery of a SCFA biotherapy. This was accompanied by a shift in fecal and circulating metabolites involved in the glutamate, arginine, butanoate, purine, pyrimidine, and tryptophan pathways. We then demonstrated that transplantation of the post-biotherapy fecal microbiota from butyrate responder participants delayed diabetes onset in germ-free NOD mice. Diabetes protection was associated with altered arginine, glutamate, purine, pyrimidine and tryptophan metabolism, similar to the pathways enriched in the human study. Within the mouse gut tissues of the diabetes-protected mice, IgG antibody, B-cell responses, and inflammatory innate immunity-related genes were downregulated while aryl-hydrocarbon receptor ligand activity and IgA were increased. Aryl-hydrocarbon receptor ligand activity and microbial markers correlated with measures of glycemic control in the patients. These data provide mechanistic insights into how a unique polysaccharide enriched with SCFAs acetate and butyrate, may interact with the host via intermediary metabolites to enhance mucosal immunity, impact the gut barrier, and protect from autoimmune diabetes.

Using fecal proteomics allowed us to study the local host response to SCFA-biotherapy. Within the human proteins altered after the intervention, there was a strong signature related to neutrophils and myeloid cells as well as epithelial junction proteins and reduced cell-death pathways. Anterior gradient protein homolog-2 (AGR2), which increased after the intervention, protects goblet cells from endoplasmic reticulum stress and is required for the production and processing of gel-forming mucins[28]. Together, this suggests that the impact of neutrophils in the gut epithelium following the biotherapy is not cytotoxic or damaging to the gut epithelium. Neutrophil proteins that increased included MMP9 and CD11b, which are characteristic of tertiary neutrophil granules. Tertiary granules are much less cytotoxic than primary/azurophilic neutrophil granules and, in some circumstances can be regulatory and involved in resolution of inflammation[29]. Neutrophil-produced inflammatory proteins such as calprotectin, MPO and neutrophil elastase did not change after SCFA-biotherapy. MMP9 is a protease that facilitates transmigration of neutrophils into tissue[30]. Transmigrating neutrophils can enhance mucosal epithelium healing and resolution of inflammation via localized oxygen depletion[31]. Our pathway analysis showed an enrichment of antioxidant proteins related to response to hypoxia and cell redox homeostasis. Butyrate is known to stabilize hypoxia-inducible factors, aiding in maintaining a low-oxygen environment found in a healthy colonic epithelium[32]. High MMP9 expression is also characteristic of proangiogenic neutrophils, important for revascularization of hypoxic sites[33]. Restriction of oxygen availability in the gut is one mechanism the host uses to favor growth of beneficial anaerobic bacteria and restrict pathobionts[34]. Hence, regulation of oxygen levels in the intestinal epithelium may be an event downstream of SCFA-biotherapy, mediated by neutrophils and butyrate.

N2 neutrophils are a subpopulation involved in tissue repair responses and are characterized by expression of MMP9, NOS2, ARG-1, TGF-β, and IL-10[35]. Polarization between pro - and anti-inflammatory immune subsets is heavily driven by arginine availability, with low arginine considered anti-inflammatory. NOS2 and ARG-1 are both downstream of ASS1 and part of the urea cycle and arginine metabolism pathways enriched in the human stool proteome, and metagenomics datasets. ASS1, the rate-limiting step in arginine biosynthesis, increased following SCFA-biotherapy and persisted after the washout period. Both NOS2 (which was strongly increased at 6 weeks), and ARG-1 degrade arginine, reducing its bioavailability. N2 neutrophils, similar to M2 macrophages, deplete arginine by converting it into NO, ornithine, proline, and polyamines, pathways involved in wound repair and regulating immunity[36]. Arginine starvation suppresses T cell proliferation via multiple mechanisms, including CD3ζ downregulation[36,37]. Arginine was decreased in the diabetes-protected mice, and creatine, a product of arginine degradation that promotes M2 macrophage polarization[38], was elevated in the human fecal metabolome. Production of NO via NOS2 is another immunosuppressive mediator that reduces T-cell activation via nitration of T-cell receptors and MHC molecules[39,40]. Although excessive NO from the host, when converted to nitrate, can drive the expansion of facultative anaerobic bacteria contributing to dysbiosis[41], we did not observe increases in dysbiotic bacteria[19].

Our data demonstrated that arginine metabolism in both the microbiota and host was activated following SCFA-biotherapy. In a large cohort study of children at risk for T1D (the TEDDY study), control subjects that did not progress to T1D or islet autoimmunity had a higher abundance of arginine and ornithine degradation, arginine biosynthesis and fermentation pathways within their microbiota[5]. In our mouse model, we observed lower fecal ornithine and arginine in the mice with delayed diabetes progression. In NOD mice, an inhibitor of conversion of arginine to ornithine by arginase-1 has been shown to protect against diabetes progression[42]. In vivo, ornithine is a major precursor for polyamines such as putrescine, spermidine, and spermine. Polyamines are increased in multiple autoimmune diseases and are important in T-cell immunity[43]. Within beta cells, polyamines are thought to contribute to endoplasmic reticulum and oxidative stress and play a role in islet inflammation[44]. Spermidine supplementation led to a higher incidence of diabetes in NOD mice[45]. Alpha-difluoromethylornithine (DFMO), an inhibitor of the enzyme that converts ornithine to polyamines, delayed the onset of experimental autoimmune encephalomyelitis[46]. In a recent phase I clinical trial in recent-onset T1D, DFMO showed preliminary evidence of preserving C-peptide at 6 months following treatment[47] and is currently being trialed in a phase-2 study (NCT05594563).

https://doi.org/10.1038/s41467-025-58319-y

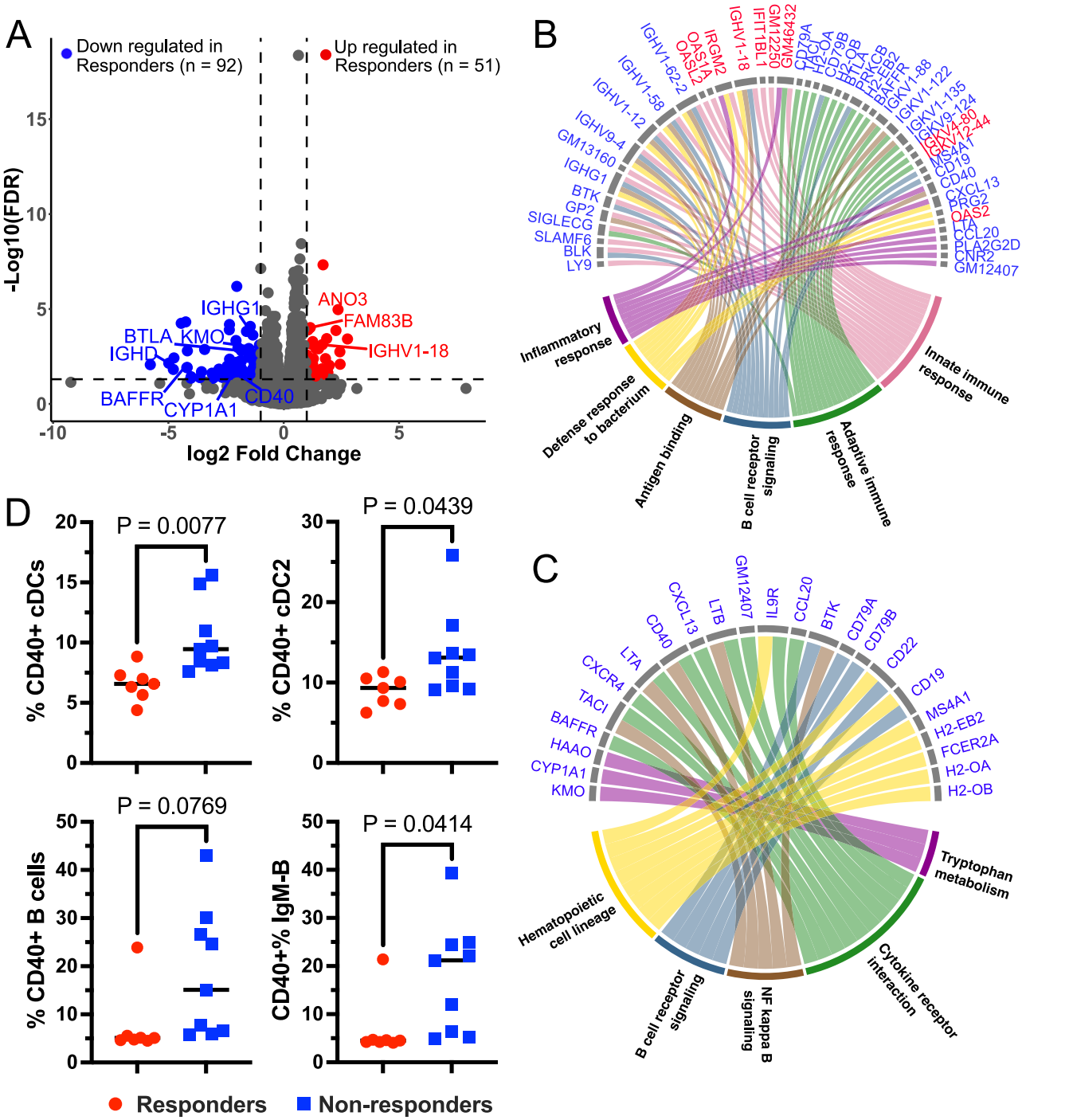

Fig. 6 | Ileal changes in B-cell, innate immunity, and tryptophan metabolism gene signature in responder-microbiota colonized mice. A RNA sequencing of ileum tissue from offspring of mice colonized with 6-week samples from SCFA-biotherapy responder (donor C, $n = 4$) and non-responder (donor B, n = 4) mice, collected at 10 weeks of age. Volcano plot of differentially expressed genes in the ileum. Significance determined using Bioconducter package DESeq2 (two-sided analysis). Selected pathways enriched between responders and non-responders in the ileum using **B** Gene Ontology and **C** KEGG. Red labels: genes increased in responders, blue labels: genes decreased in responders. **D** CD40 expression on conventional dendritic cells (cDCs), CD11b + XCR1- dendritic cells (cDC2), total B cells, and IgM- B cells in the spleens of the responder ($n = 7$) and non-responder ($n = 9$) mice at 10 weeks of age. The gating strategy is shown in Supplementary Fig. 12. Data pooled from two experiments. The line represents median value. Significance was determined using an unpaired, two-tailed t-test. See also Supplementary Data 13–15.

The tryptophan metabolism pathway in the plasma was significantly enriched at follow-up. The gut microbiota transforms dietary tryptophan into indole derivatives like indolelactic acid and indole-pyruvate. These compounds serve as ligands for the Ahr, a pivotal pathway in preserving intestinal equilibrium and immune tolerance[48]. Tryptophan is also metabolized by the host enzyme IDO to produce kynurenine, which contributes to the tryptophan pathway enrichment in plasma at follow-up. IDO activity was reported to be reduced in children with T1D[49]. Microbial producers of indolelactic acid include *Parabacteroides distasonis*, *Bacteroides ovatus*, and *Bifidobacterium adolescentis*[50], all of which increased in our study participants after the intervention[19]. In our mouse model, tryptophan metabolites quinic

https://doi.org/10.1038/s41467-025-58319-y

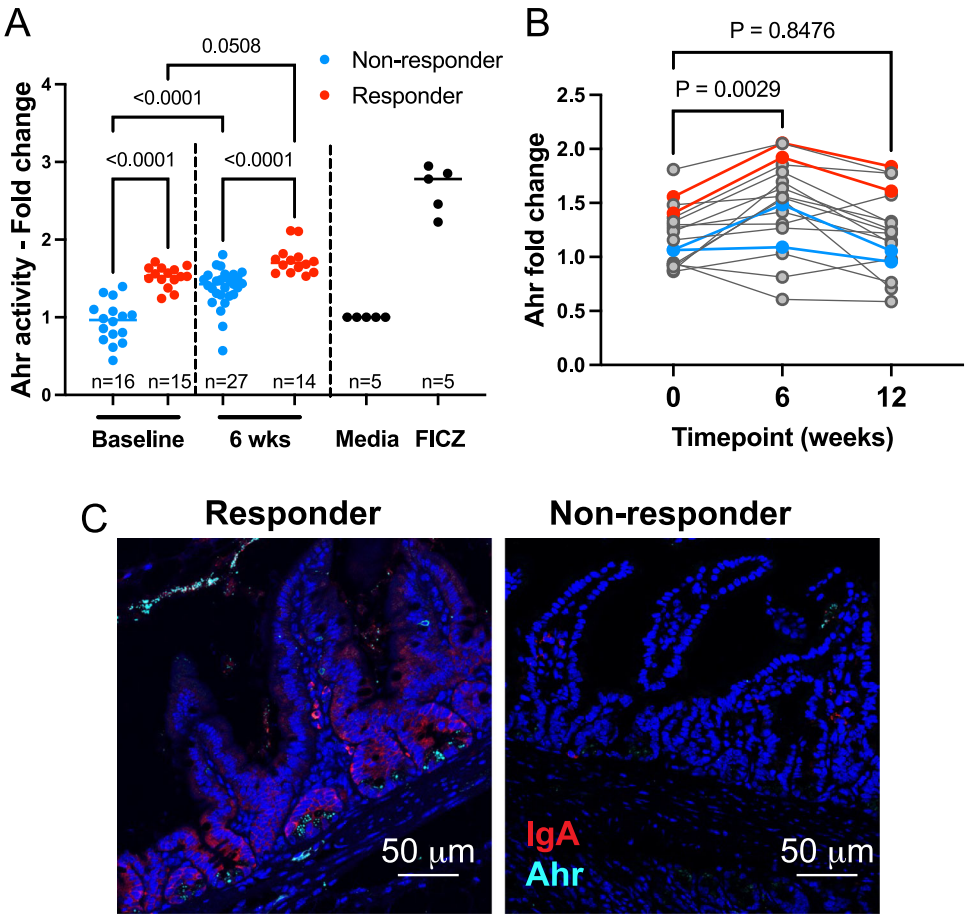

Fig. 7 | Enhanced aryl-hydrocarbon receptor activity in responder-microbiota colonized mice. A Fecal water extract from human-microbiota colonized mouse offspring at 7–10 weeks of age was used to stimulate Ahr luciferase reporter cells. Significance was determined by one-way ANOVA with Sidak's correction (two-sided). Data was pooled from two experiments. **B** Fecal water extract from the human study participants ($n = 18$) was used to stimulate Ahr luciferase reporter cells. Human donors used in the mouse study were indicated by colors (non-responder donors – blue, responder donors – red). FICZ synthetic Ahr ligand was used as a positive control and data is expressed as fold change relative to unstimulated cells. Significance determined by repeated-measures one-way ANOVA with Dunnett's correction (two-sided). **C** Representative images of ileum tissue from human-microbiota colonized mouse offspring at 10 weeks of age stained with anti-IgA (red), anti-Ahr (cyan), and DAPI (blue). Image representative of staining from $n = 5$ responder and $n = 6$ non-responder mice from one experiment.

acid and xanthurenic acid were higher in the feces of responder mice. Quinic acid is metabolized in the gastrointestinal tract leading to increased systemic tryptophan availability[51]. Quinic acid in serum was also reported to be decreased in children that rapidly progressed to T1D compared with slow progressors[14]. Xanthurenic acid is an Ahr ligand downstream of kynurenine, and usually considered an endogenous tryptophan metabolite[52]. However, certain gut bacteria can also metabolize kynurenine pathway intermediates into xanthurenic acid[53]. Xanthurenic acid is lower in inflammatory bowel disease patients, and xanthurenic acid reduced colitis symptoms and inflammation in animal models and promoted epithelial repair[26]. However, the role of these metabolites in type 1 diabetes remains to be explored.

Gene expression analysis of the ileum tissue identified upregulation of *Cyp1a1* in the diabetes-susceptible/non-responder group. While *Cyp1a1* is upregulated by Ahr signaling, it acts as a negative regulator of Ahr by depleting Ahr ligands[25]. Our Ahr reporter assay demonstrated that the post-SCFA-biotherapy microbiota had higher Ahr stimulatory activity and that Ahr itself was upregulated in the ileum tissue. Administration of synthetic Ahr ligands in NOD mice have been shown to reduce insulitis and protect from diabetes via effects on both $Foxp3^+$ Tregs and $ROR\gamma t^+$ T cell populations[54,55]. Similarly, administration of a diet yielding butyrate or acetate or a combination protected NOD mice from diabetes and islet autoimmunity[4,56], as well as protecting mice from gut infection[57]. With the combination of both acetate and butyrate metabolites attached to a polysaccharide biomolecule has a more potent and synergistic immunomodulatory effect for diabetes protection. Thus, our data indicate that SCFA-biotherapy may induce multiple beneficial metabolic pathways.

Our analysis of the intestinal tissue indicated a potent upregulation of B-cell-related genes in the non-responder mice, including *IghG1* and *IghG3* antibody heavy chain genes, whereas IgA protein was increased in the responder ileum tissue. Microbiota-specific IgG production and FcγR activation by IgG is considered inflammatory within the intestinal mucosa and associated with ulcerative colitis, while mucosal IgA is associated with homeostasis[58]. Both acetate and butyrate have been shown to promote intestinal IgA production, in particular butyrate promotes lower-affinity, T-cell-independent IgA production[57,59,60]. The T-cell-independent IgA pathway tends to recognize conserved microbial antigens such as LPS, whereas T-dependent IgA leads to class-switching and high-affinity antibody responses. The enrichment of pathways such as "response to lipopolysaccharide", "defense response to bacterium" and "inflammatory response" in the ileum tissue of the non-responder colonized mice suggests there was a qualitatively different environment that may have been promoting more potent immune activation. People with T1D had a higher proportion of IgA-coated bacteria, suggesting increased high-affinity IgA produced by class-switching, and this negatively correlated with SCFA levels[7]. In our proteomics analysis of the human stool

https://doi.org/10.1038/s41467-025-58319-y

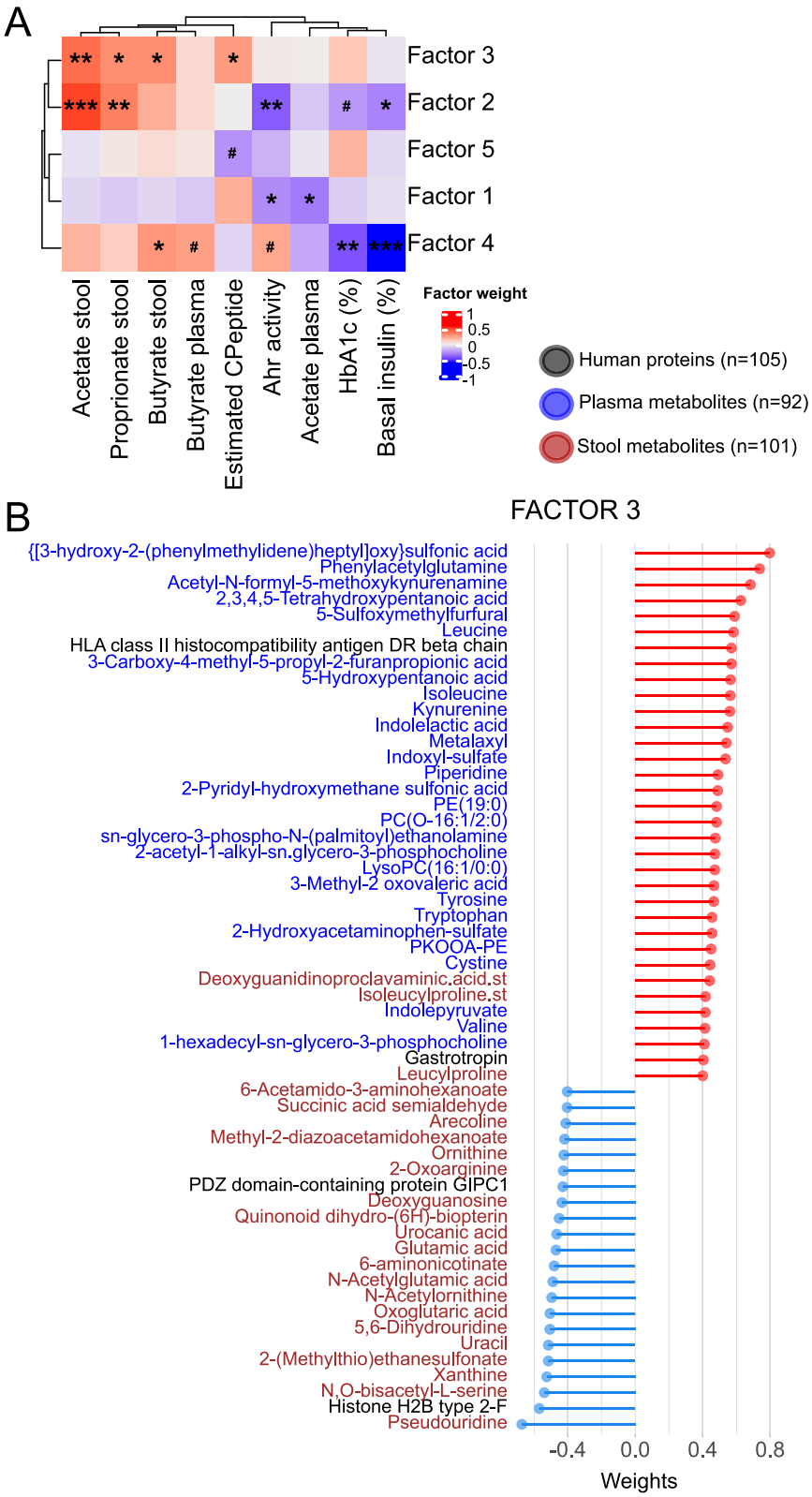

Fig. 8 | Multi-omic factor analyses (MOFA) identify latent factors associated with glycaemic control, SCFA, and Ahr activity. MOFA was used to integrate bacterial taxa ($n = 22$), bacterial pathways ($n = 91$), human stool proteins ($n = 101$), stool metabolite ($n = 101$) and plasma metabolite ($n = 92$) datasets. The identified latent factors were correlated with clinical data, SCFA and Ahr activity. **A** Heatmap indicating two-sided Pearson's correlation between clinical variables and model factors. $^{***}P < 0.001$, $^{**}P < 0.01$, $^{*}P < 0.05$. **B** Variables contributing to latent factor 3. Only variables with absolute weight >0.4 are included in the plots. Black text: human proteins, blue text: plasma metabolites, red text: stool metabolites.

samples, multiple antibodies changed in abundance across time, with some up and some downregulated. However, untargeted proteomics is not able to resolve the class of these antibodies. Thus, while butyrate production in our mouse model likely reduced mucosal IgG and increased IgA production, this mechanism still needs to be confirmed in human studies.

Our study had several limitations related to the single-arm, open-label design and small sample size of our pilot human study. Our fecal proteomic analysis could not identify the source of the proteins detected, which may be derived from the any part of the intestine, the pancreas or another organ. Only proteins with a relatively high abundance were detected by our untargeted proteomics approach, and many biologically relevant low-abundance proteins will be missed. We also did not directly assess gut barrier function via intestinal permeability assessment in the study participants Likewise, our metabolomics analysis could be followed up with a targeted analysis for pathways of interest. While human fecal microbiota transfer is considered one of the best approaches for establishing disease causality[61], this model has limitations. Only a proportion of the human microbiota colonized the mice, and those that did colonize changed in abundance compared to the donor samples, likely due to the different mouse diet, housing and physiology or preservation method of the stool samples. Some important taxa colonized the mothers but did not transmit well to the offspring (e.g., *Faecalibacterium*). However, we observed a functional replication in the mouse of the human donor butyrate response and metabolite profiles.

We demonstrated that after undergoing SCFA-yielding biotherapy, adults with T1D show changes in the gut epithelium, mucosal immunity, and production of a range of metabolites. A functional shift in the gut microbiota drives enhanced amino acid and nucleotide metabolism both locally and systemically, particularly arginine, glutamate, purine, pyrimidine and tryptophan-related metabolites. Purine and pyrimidine metabolites correlated with markers of glycemic control. We were then able to link these changes in the human system with reduced diabetes progression using our mouse microbiome transfer model. Our analysis shows changes in the mucosal immune response after administering SCFAs were linked to the metabolism of purine, pyrimidine, arginine, glutamate, and tryptophan, as well as the anti-inflammatory effects of Ahr ligands. These changes were related to measures of glycemic control, suggesting a potential for clinical benefit. Here, we have uncovered that a specialized acetate-butyrate-yielding biotherapy positively impacts the production of beneficial downstream metabolites, indicating the wide-ranging potential of SCFAs in the slowing, halting, or reversing the progression of T1D.

Methods

Study participants

Participants in this study were adults with T1D who had previously been described in a single-arm trial using an oral intervention consisting of a polysaccharide biomolecule modified with acetate and butyrate, also known as HAMSAB[19], (Fig. 1A). The trial protocol was approved by the Sydney Local Health District Human Research Ethics Committee, the Human Research Ethics Committees of Monash University and University of Queensland (lead approval HREC/18/RPAH/241) and complies with all relevant ethical regulations. All patients provided written informed consent for the use of their samples and data in this study. The trial was registered with Australia New Zealand Clinical Trials Registry (ACTRN12618001391268). The trial participants were aged 18–45 years, had a clinical diagnosis of T1D <6 months and HbA1c ≤ 8.5% (Supplementary Data 1). Estimated C-peptide was calculated as described using age, gender, HbA1c, insulin dose and body mass index[62]. All available stool and plasma samples were used in this study from the $n = 21$ participants collected at baseline ($n = 20$ stool and $n = 18$ plasma samples), 6 weeks ($n = 18$ stool and plasma samples), at the end of the supplementation period and 12 weeks ($n = 18$ stool and plasma samples), after a 6-week washout[19]. Additional approval for re-use of the participant stool samples for mouse colonization experiments was obtained from the University of Queensland Human Research Ethics Committee (low and negligible risk approval 2023/HE000166).

Mice

NOD/ShiLtJArc (NOD) mice were originally obtained from the Animal Resource Facility (Perth, WA, Australia) and rederived into the Translational Research Facility Gnotobiotic Facility, within the Biological Resources Facility, University of Queensland. The germ-free NOD breeding colony was maintained on an autoclaved Teklad 2019S diet (Catalogue #2019S, Inotiv, Lafayette IN, USA) and all experimental mice were maintained on NIH07 autoclaved diet Catalog #7922, Inotiv) fed ad libitum. Sterile water was provided ad libitum. Germ-free mice were housed within sterile isolators with a 12-h light/dark cycle, 22 °C. 67–72 median relative humidity. Following colonization with a complex human microbiota, experimental mice were housed in sterilized Tecniplast (Varese, Italy) individual isolator cages. Only female offspring of colonized mice were used for experiments. All experimental procedures were performed in sterile conditions within a biosafety cabinet. All experiments were approved by the University of Queensland Animal Ethics Committee (2021/AE000553).

Human microbiota transfer into germ-free mice

Baseline and 6-week stool samples from four trial participants were selected based on donor fecal butyrate response. Stool samples were processed within an anerobic chamber. Anaerobic glycerol solution (phosphate-buffered saline containing 12% glycerol and 0.1% Cysteine) was added to human stool and passed through a 70 µm cell strainer. The live bacterial cell count was determined using a BacLight Bacterial Viability Kit (Thermo Fisher Scientific, Waltham, MA). Germ-free NOD/Lt females (6 weeks of age) were gavaged on day 0 with 1.2×10^7 live bacteria (from a single donor sample) or sterile PBS and with 2.4×10^7 live bacteria 7 days later. The colonized females were mated with germ-free NOD males 7-days after the second gavage. Female offspring were monitored weekly for diabetes onset starting at 10 weeks of age via blood glucose testing from tail-vein blood collected by sterile pipette and tested with a Freestyle Optium Blood Glucose Monitoring device (Abbott). Mice were deemed diabetic after two consecutive readings of >16 mmol/L. The stool was collected from mothers at week 2 and from offspring at 5 and 11 weeks for 16s rRNA gene amplicon sequencing analyses and at weeks 7 and 9 for metabolite analyses.

Stool protein extraction, digestion and purification for proteomics

Human stool samples were resuspended in 3:1 (w/v) of ice-cold potassium phosphate buffer (50 mM containing 5 mM EDTA). Heavy particles were allowed to settle by incubating on ice for 30 min and the supernatant retained. Bacteria and debris were pelleted by centrifuging at 8000 *g* for 10 min at 4 °C. The soluble fraction, which is enriched for human proteins[20], was then removed and re-spun at 8000 *g* for 10 min at 4 °C and the supernatant was used for both proteomics and metabolomics analysis (see below). Isolated protein (20 µg as estimated by the direct detect spectrometer), was lysed in a solution containing 1% sodium deoxycholate, 10 mM tris[2-carboxyethyl]phosphine and 40 mM 2-chloroacetamide in 100 mM Tris pH 8 and boiled at 95 °C for 5 min. Proteins were digested using porcine trypsin (Promega, Madison, WI) at a protein:trypsin ratio of 50:1 (w/w) for 16 h at 37 °C. Protein digestion was halted and detergent precipitated using trifluoroacetic acid (TFA) at a final concentration of 5%. Samples were clarified by centrifugation at 13,000 × *g*. Tryptic peptides were desalted using Glygen C18 pipette tips on an Agilent Bravo liquid handler. The eluent was evaporated with centrifugation under vacuum and

tryptic peptides were resuspended into a final concentration of 0.5 µg/µL with 0.5% TFA for mass spectrometry.

Proteomic mass spectrometry and protein identification

Samples ($n = 56$) were analyzed in duplicate on a Q Exactive High-Field mass spectrometer coupled with an UltiMate 3000 UHPLC (Thermo Fisher Scientific). Tryptic peptides were loaded on a Thermo Fisher Scientific trap column 160454 (0.3 mm × 5 mm) and separated with a Thermo Fisher Scientific EASY-Spray HPLC column ES803 (75 µm × 500 mm), over a 100-min gradient from 3 to 25% acetonitrile over 60 mins followed by 25–40% acetonitrile over 12 min in buffer containing 0.1% formic acid at a flow rate of 250 nL/min. The columns were washed with 95% acetonitrile for 15 min and re-equilibrated with 3% acetonitrile for 7 mins. Survey scans were acquired from 375m/z–1500m/z with a resolution of 60,000, automatic gain control of 3×10^6, and maximum injection time of 50 ms. Precursor ions consisting of the top 20 most intense ions were selected for tandem mass spectrometry and fragmented with a normalized collision energy of 28%. Dynamic exclusion was set to 20 s, and the mass exclusion width of 10 parts per million. Second stage of mass spectrometry was acquired with between 200m/z–2000m/z at a resolution of 15,000, automatic gain control of 5×10^5, and maximum injection time of 20 ms.

Human peptides and proteins were identified and quantified using Proteome Discoverer (v2.5.0.400, Thermo Fisher Scientific), which applies label-free quantification methods. Search parameters included carbamidomethylating of cysteine and deamidation of asparagine as fixed and variable modifications respectively. A maximum of two missed cleavages were allowed and the false discovery rate was set at 0.01. Proteins were searched against the UniProt human database. Common contaminants identified by MaxQuant (v2.3.2.0, Max-Planck-Institute of Biochemistry) were removed.

Proteomics data processing

Protein intensities from duplicate samples were averaged. Proteins that were not present in a minimum of 40% of a single timepoint were excluded. A multiple mixed imputation strategy was implemented using R package, imp4p[63]. Here, the likelihood of a protein to be "missing completely at random" (MCAR) or "Missing not at random" (MNAR) is predicted using Bayesian probabilities. Proteins identified as MNAR were imputed using 'Imputation under a Gaussian Complete Data Assumption', and those determined as MCAR were imputed using random forest. Intensities were subsequently log2 transformed and normalized using variance stabilization (R package "vsn") before linear mixed model analysis using R package 'lme4'.

Fecal and plasma metabolite sample preparation

Metabolites were analyzed from plasma (25 µL, $N = 54$), mouse fecal pellets (0.2 g, $N = 39$) or the enriched human soluble stool fraction ($N = 56$) prepared for proteomics (see above). Plasma samples were prepared at 4 °C by the addition of ice-cold 200 µL of 1:1 acetonitrile:methanol was added and mixed for 20 min. Subsequently, samples were centrifuged at 22,000 × g for 10 min and the supernatant remove for further analyses. For mouse fecal pellets, 1 mL of 50% acetonitrile was added and homogenized with metal beads for 10 min at 30 Hz (Retsch Mixer Mill MM400) at 4 °C. Homogenate was then centrifuged at 16,000 × g for 10 min at 4 °C and the supernatant removed and diluted with 50% acetonitrile until the concentration was 2 mg dry weight/mL. Mouse fecal homogenate was used for untargeted metabolomics and SCFA quantification (see below). The enriched human soluble stool fraction only required protein and salt removal. Proteins and salts were removed from human fecal supernatants, mouse fecal homogenates or plasma by adding cold extraction solvent containing methanol spiked with the fully isotopically labeled internal standards (1:1000) 13 C,15N-amino acid mixture (Cell Free Amino Acid Mixture - 13C,15N, Merck, Rahway, NJ, USA), 1 µM of buffers N-cyclohexyl-3-aminopropanesulfonic acid, (3-((3-cholamidopropyl) dimethylammonio)-1-propanesulfonate, piperazine-N,N′-bis(2-ethanesulfonic acid) and 2 µM of the antioxidant butylated hydroxytoluene, and incubating at 4 °C for 1 h. Following centrifugation at 14,000 × g for 10 min, supernatants were transferred to an LC/MS vial for analysis and 10 µL injected into LCMS (1 injection per sample).

Metabolomics LC-MS analysis

LCMS analysis was performed by the Monash Proteomics and Metabolomics Platform and acquired on Q-Exactive Orbitrap mass spectrometer (Thermo Fisher Scientific) coupled with a Dionex Ultimate® 3000 RS HPLC system (Thermo Fisher Scientific). Chromatographic separation was performed on a ZIC-pHILIC column (5 µM, polymeric, 150 × 4.6 mm, SeQuant®, Merck) with buffer A as 20 mM ammonium carbonate and buffer B acetonitrile, with HPLC and MS settings as previously described[64]. Flow rate was set to 0.3 mL/min, gradient was as follows: 0 min 80% B, 15 min 50% B, 18 min 5% B, 21 min 5% B, 24 min 80% B and 32 min 80% B. Column compartment temperature was 25 °C and autosampler temperature was 4 °C. Heated electrospray ionization (HESI) source parameters were: sheath gas 50, aux gas 20, sweep gas 2 arbitrary units, capillary temperature 300 °C, S-lens RF level 50, aux gas temperature 120 °C, spray voltage 4.0 kV in positive mode, 3.5 kV in negative mode. MS data was collected in full scan mode with positive and negative polarity switching over 85 – 1275 m/z range, at 35k resolution, with 1e6 AGC and 50 ms maximum injection time. A pooled sample was used to acquire MS2 data for ID purposes in DDA mode in positive and negative ion detection modes as separate injections. Samples were analyzed in randomized order and pooled quality control samples were analyzed throughout each batch to confirm method reproducibility. Mixtures of pure authentic reference standards containing over 320 metabolites[64] were acquired as separate injections before each study and used to confirm retention times to assist with metabolite identification.

Metabolomics data processing

The acquired LCMS data was processed in untargeted fashion using open source software IDOEM[65]. The standard IDEOM workflow with default parameters was used to detect and group peaks, eliminate unwanted noise and artefacts, and identify and quantify metabolites, as previously described[64]. Metabolites were identified by searching against the IDEOM database based on accurate mass and retention time (from authentic standards analyzed in the same batch) for Metabolomics Standards Initiative level 1 metabolites. Where authentic standards were not available, putative metabolite identities are annotated (Metabolomics Standards Initiative level 2) based on predicted retention time[66]. Annotated metabolites were inspected for peak quality and the following additional data filters were applied: When a metabolite was identified more than once, mass and retention times were inspected to select the most likely peak corresponding to that metabolite (based on chromatographic behavior of the authentic standards). Metabolites with an average peak intensity of less than 500,000 were removed to reduce the likelihood of LC-MS artefacts being misidentified as metabolites. Metabolites that were not present in at least 40% of samples for a single timepoint were removed. Metabolites with less than two missing values were imputed with the average value from the timepoint. The remaining metabolites were log2 transformed and normalized using variance stabilization methods in the R package 'vsn' before linear mixed model analysis using R package 'lme4', similar to proteomic samples. Correlations between stool metabolites that were significantly altered after the SCFA biotherapy (FDR < 0.01) and glycaemic variables estimated C-peptide and glycated hemoglobin (Hb1Ac) was performed using repeated measures correlation

(R package rmcorr). Correlation p-values were adjusted for multiple correction using FDR.

Peak areas of tryptophan pathway metabolites were obtained by searching metabolomics raw data using the Tracefinder application (Thermo Fisher Scientific). Tryptophan metabolites that were detected and integrated were: 2,8-dihydroxyquinoline, indole-3-propionic acid, indole acetic acid, indole lactic acid, kynurenine, tryptophan and xanthurenic acid. Identities of these features were confirmed with reference standards or MS2 spectrum and 3 ppm mass error cut off was used. Other metabolites searched for but not found: 1H-indole-3-carboxaldehyde, 3-methyl-2-oxindole, 3-methylindole, indole,indole-3-acrylic acid, indole-3-carboxylic acid, kynurenic acid. Spectral identification information for tryptophan metabolites is provided in Supplementary Data 18.

SCFA quantification on mouse fecal samples

A liquid chromatography-multiple reaction monitoring mass spectrometry (LC/MRM-MS) method measuring 76 transitions from 11 nitrophenylhydrazine (NPH)-derivatised SCFAs (Supplementary Data 18) was developed based on[67,68]. Method development is detailed in the Supplementary Methods. Mouse feces (2 mg dry weight/mL), calibration standards, blank and a pooled quality control sample were derivatised with 3-NPH, and then mixed with an isotope-labeled internal standard solution prepared using $^{13}C_6$-3-NPH·HCl (Cayman Chemical, Ann Arbor, Michigan) prior to LC-MS analysis in negative ionization mode on a 1290 Infinity II UHPLC coupled to a 6470 QQQ mass spectrometer (Agilent, Santa Clara, USA). Samples ($n = 108$) were analyzed in a randomized order bracketed by quality control and calibration standards. Control groups included $n = 5$ germ-free NOD mice and $n = 10$ SPF NOD mice. Skyline[69] was used for peak picking, integration, and calibration curve construction, while downstream calculations were performed in Excel. SCFA transitions are shown in Supplementary Data 18.

Mouse stool DNA extraction and 16 s rRNA library preparation

DNA from mouse feces was extracted using 3:1 ratio of 0.1 mm +1 mm Zirconia beads (Daintree Scientific) in lysis buffer (50 mM Tris-HCl, 500 mM NaCl, 50 mM EDTA, 4% SDS). Samples were homogenized using a Precellys 24 (Bertin Technologies) and then supernatants then treated with RNAse and then Proteinase K. DNA was subsequently extracted using the automated Maxwell 16 LEV Blood DNA extraction kit (Promega, Madison, WI). Variable region V6-V8 were amplified using the Illumina-seq-926F (AAACTYAAAK-GAATTGRCGG) and 1392R2 (ACGGGCGGTGWGTRC) primers with Nextera XT (Illumina) adapter sequences[70]. Amplicon sequences were purified using E-gels. Indexed amplicon libraries were then purified using AMPure XP beads (Beckman Coulter, Brea, CA, USA), pooled to an equimolar concentration of 10 nM. Sequencing was performed by the Australian Centre for Ecogenomics (University of Queensland, Brisbane, Australia) using an Illumina MiSeq using the MiSeq V3 chemistry (2x 300 bp) according to the manufacturers protocol.

16s Amplicon data processing

16s rRNA amplicon sequences were demultiplexed and preprocessing performed using '[71]. Primer sequences were removed from forward demultiplexed reads using q2-cutadapt plugin. Amplicon sequences were denoised and trimmed to 250 bp using dada2 plugin. Taxonomy was assigned using a classifier trained on V6 – V8 16 s region of the 16S SILVA database (release 138, clustered at 99% identity). Generated amplicon sequence variant taxonomic tables were analyzed and compared at the genus level. Taxa present in two or less mice or had a minimum abundance <0.01% were removed from analyses. Bacterial counts were rarefied at 15,000 and normalized using center log-ratio with an offset of 1. Differences in microbiome taxonomic composition between responder groups from donor 6-week trial stool samples were determined using ANOVA.

RNA sequencing on mouse intestinal tissue

Colon and ileum were collected in RNAlater Stabilization Reagent (Thermofischer Scientific). Total RNA was extracted with RNeasy Mini Kit (Qiagen). Transcriptomics sequencing analysis was performed by Azenta Life Sciences using Illumina paired end 2×150 base pair configuration using an Illumina NovaSeq platform to a depth of 79-95 million reads per sample. Raw transcripts were inspected for quality control using FastQC (version 0.10.1) with the average quality score for each transcript above 30. Adapter sequences and sequences with <75 bases were removed using Cutadapt (version 1.9.1). Transcripts were aligned to the reference genome Mus Musculus using Hisat (version 2.01).

Flow cytometry

Single-cell suspensions were prepared from spleen and lymph nodes by passing cells through a 70-micron cell strainer (BD Biosciences, Franklin Lakes, NJ). Red blood cells in spleen were lysed with ACK lysing buffer. Cells were stained for surface and/or intracellular markers in the dark at 4°C. T-cells were phenotyped using anti-mouse antibodies CD8-BUV805 (Clone 53-6-7, 1:400), CD4-BUV496 (GK1.5, 1:400), CD44-BUV395 (IM7, 1:400) from BD Biosciences, CD279 (PD-1)-BV711 (29 F.1A12, 1:400), CD152(CTLA4)-BV605(UC10-4B9, 1:200) from (BioLegend, San Diego, CA, USA), FoxP3-PE-Cy5 (FJK-16s, eBioscience, 1:400). I-A^{g7}- BDC2.5mim monomers specific for islet peptide were from the NIH tetramer core facility and tetramerized with streptavidin-PE (Prozyme, Seattle, WA, USA) as described[72]. Dead cells were excluded with FVS440 for live/dead stain from BD Biosciences. Antigen presenting cells were phenotyped using anti-mouse antibodies CD80-PE (16-10A1, 1:800), CD40-PE-Cy7 (3/23, 1:400), CD11c-BV605 (N418, 1:200), I-A^{d}-AF647 (39-10-8, 1:400), H-2Kd-FITC (SF1-1.1, 1:200), XCR1-BV650 (zet, 1:200), TCR-APC Fire750 (H57-597, 1:400), CD19-PerCP-Cy5.5 (6D5, 1:200), CD274 (PDL1)-BV785 (10 F,9G2, 1:200) from Biolegend. CD11b-BUV395 (M1/70, 1:200), CD86-BV510 (GL1, 1:200), IgM-BV421(UCH-B1, 1:200) from BD Biosience and Aqua for dead cell exclusion (Thermofisher Scientific, Waltham, MA, USA). Flow cytometry was performed using a BD FACSymphony A5 using FACS DiVa 8.0.1 software and data analyzed using FlowJo V10.8.1 software (Tree Star, Ashland, OR, USA). Gating strategy is shown in Figs. S6 and S12.

Ahr reporter cell assay

HT29 cells (ATCC HTB-38) were transduced with lentivirus carrying Ahr with firefly luciferase reporter (Ahr vector # 90337, with enveloping and packaging vectors pCMV-VSV-G #8454 and pCMV-dR8.2 dvpr # 8455 all from addgene, Waterton MA, USA). HT29 Ahr reporter cells (50,000) were plated on white 96 well plate in complete media (DMEM supplemented with 10% FBS, 1% Penicillin Streptomycin, and 1% Glutamine) and incubated at 37 °C overnight. Next day, cells were treated with 10% v/v of fecal water (as prepared for proteomics) for 4 h. 6-Formylindolo[3,2-b]carbazole (FICZ, 100 nM, Sigma-Aldrich) was used as a positive control. Luciferase assay was performed using Pierce™ Firefly Luciferase Glow Assay kit (Thermofisher). Ahr activity was normalized to cells only control and presented as fold change.

Insulitis and immunofluorescence staining

Pancreata were fixed in 10% neutral buffered formalin (Sigma-Aldrich, St Louis, MO, USA) and stained using hematoxylin and eosin. Slides were scanned using an Olympus VS120. Insulitis were assessed as follows: 0 = no infiltration, 1 = peri-insulitis, 2 = mild insulitis (<50% of islet infiltration), 3 = severe insulitis (>50% of islet is affected by pathological change), 4 = complete infiltration. A minimum of 30 islets were scored per pancreas using blinded analysis. For immunofluorescence, pancreas sections were stained with anti-insulin (Clone #182410,

1:2000, from R&D Systems, Minneapolis, MN, USA), anti-glucagon (Clone ICACLS, 1:500, from eBiosiences). Secondary antibodies donkey anti-rat AF488 and donkey anti-mouse AF647 (Invitrogen, used at 1:500) and DAPI to further identify residual islets. Slides were scanned on Olympus VS200 and exported to Image J for analysis.

Ileum and colon tissue were rolled and fixed in 10% neutral buffered formalin before processing in paraffin blocks. Paraffin sections were rehydrated then antigens retrieved with citrate buffer. Sections were permeabilized with 0.5% Triton-100, followed by serum blocking. Primary antibodies were goat polyclonal anti-mouse IgA-UNLB (1:500) and Ahr monoclonal (Clone RPT1, 1:150) antibody, and secondary antibodies were Donkey anti Goat Alexa Fluor®568 and Donkey anti Mouse Alexa Fluor®647 (both used at 1:500) with DAPI nuclei staining. Fluorescence images were acquired using Confocal Microscope Olympus FV3000.

Statistical analysis

Changes in multivariate signatures of each 'omic dataset across timepoints were investigated using supervised Partial-Least-Squares Discriminant-Analyses (PLS-DA) and unsupervised Principal Component Analyses (PCA) using the R software package, mixOmics (V6.23.2)[73]. Significance was determined using Permutation Analysis of Variance adjusted for repeated measures (PERMANOVA) using the R package vegan (V2.6-6)[74]. Pairwise differences were determined using pairwiseAdonis package (V0.4) and adjusted for multiple comparisons using false discovery rate. Significant differences in individual stool proteins, plasma and stool metabolites were inferred using linear mixed models in the R package lme4 (V1.1-31). Timepoints was accounted as a random factor. Statistical significance was defined based on Likelihood Ratio Test ($p < 0.05$), with Benjamini-Hochberg correction for multiple testing. Tukey HSD test determined pairwise differences between timepoints[75]. Proteins with global $p < 0.05$ were explored for pathway enrichment (KEGG and GO:Biological Processes). Separate pathway enrichment analyses were performed on proteins that either significantly increased or decreased ($p < 0.05$) from baseline to six weeks or baseline to follow-up using the software ShinyGo V0.77[76], with an FDR cut off of 0.05. All protein coding genes were used as background. Fecal metabolite pathway enrichment was compared using MetOrigin (V1.0)[77]. Differences were determined using paired *t*-test of individual metabolites with a cut-off value of $p < 0.05$. Metabolite Pathway Enrichment Analyses (MPEA) was determined using an 'origin' based approach where identified metabolites are searched against three databases: host-only (human KEGG pathways), microbial only (all KEGG bacterial pathways) or combined host/microbe. Identified metabolites are compared with all other pathway associated metabolites in each origin-based database. Foldchange analyses confirmed directional changes of significantly different metabolites between groups. Plasma metabolite enrichment analysis was conducted using web-based MetaboAnalyst v5.0. Significant metabolites identified under linear mixed models ($p < 0.05$) were selected for the enrichment analysis (mapping to the pathway-based KEGG metabolite set library).

RNA-seq gene expression was normalized using fragments per kilo bases per million reads (FPKM). Differential gene analysis and pathway ontologies enriched in ileum and colons tissues of non-responder and responder mice were analyzed separately. Gene differential analyses on read count data was performed using Bioconductor package DESeq2 (V1.6.3) based on a model with a negative binomial distribution. Functional gene ontology analyses were performed using GOSeq with a p value threshold of 0.05[78]. Differences between stool SCFA and Ahr activity in humanized mice responders and non-responders from the different trial donor samples were compared with ANOVA and diabetes survival curves were compared using log-rank (Mantel-Cox) survival analysis using using Graphpad Prism v10.4.1.

Multiomic factor analysis

Multiomic Factor Analysis (MOFA) was performed using the MOFA2 (V3.20) R package[27]. Bacterial taxa, bacterial pathways, human stool proteins, plasma metabolites and stool metabolites were incorporated as separate "views". Bacterial taxa and pathways were from our previously published metagenomics anlaysis[19]. Variables in each dataset with $p.value < 0.05$ were selected for analyses. Each "view" was normalized as stated in the respective univariate analyses. Prior to model training, within sample variation was removed. MOFA analysis was performed with 1 analysis group using default setting except "ard factors" were set to "true" to account for the sparsity of the views.

Reporting summary

Further information on research design is available in the Nature Portfolio Reporting Summary linked to this article.

Data availability

The mass spectrometry proteomics data have been deposited to the ProteomeXchange Consortium via the PRIDE[79] partner repository with the dataset identifier PXD055787. RNAseq data has been deposited in European Nucleotide Archive with the identifier PRJEB70862. Skyline and MRM raw data for SCFA quantification in mouse stool have been deposited on PanoramaWeb (https://panoramaweb.org/HAMSABstudySCFA.url). The 16S rRNA sequencing data is available at NCBI Sequence Read Archive with accession number PRJNA1128165. Metagenomics data previously generated[19] is deposited in European Nucleotide Archive with identifier PRJEB45815. Mouse metabolomics data have been deposited in NIH Common Fund's National Metabolomics Data Repository (NMDR) website, the Metabolomics Workbench with Project ID PR002356 (https://doi.org/10.21228/M83G0N). The human metabolomics datasets generated during this study are subject to restricted access to protect intellectual property and commercial interests of the parties. Researchers from academic institutions or recognized research organizations may request access to the minimum dataset necessary to interpret, verify and extend the research by contacting the corresponding authors. Access requests must include: (1) institutional affiliation verification, (2) a signed data transfer agreement prohibiting commercial use, (3) a brief research plan outlining the intended use, and (4) confirmation of compliance with relevant ethics regulations. The review process for access requests typically takes 4–6 weeks. If approved, data will remain available to the requestor for a period of 1 year, with the possibility of extension subject to further review. Restrictions on use include prohibition of redistribution, commercial exploitation, or any use beyond what is specified in the approved research plan.

References

1. Belkaid, Y. & Harrison, O. J. Homeostatic Immunity and the microbiota. *Immunity* **46**, 562–576 (2017).
2. Craig, M. E. et al. Early-life factors contributing to type 1 diabetes. *Diabetologia* **62**, 1823–1834 (2019).
3. Siljander, H., Honkanen, J. & Knip, M. Microbiome and type 1 diabetes. *EBioMedicine* **46**, 512–521 (2019).
4. Marino, E. et al. Gut microbial metabolites limit the frequency of autoimmune T cells and protect against type 1 diabetes. *Nat. Immunol.* **18**, 552–562 (2017).
5. Vatanen, T. et al. The human gut microbiome in early-onset type 1 diabetes from the TEDDY study. *Nature* **562**, 589–594 (2018).
6. de Groot, P. F. et al. Distinct fecal and oral microbiota composition in human type 1 diabetes, an observational study. *PLoS One* **12**, e0188475 (2017).
7. Huang, J. et al. Gut microbial metabolites alter IgA immunity in type 1 diabetes. *JCI Insight* **5**, https://doi.org/10.1172/jci.insight.135718 (2020).

8. Mariño, E. SCFAs in T1D: a microbiota-targeted approach for immune tolerance. *Curr. Opin. Endocr. Metab. Res.* **24**, 100355 (2022).
9. van der Hee, B. & Wells, J. M. Microbial regulation of host physiology by short-chain fatty acids. *Trends Microbiol* **29**, 700–712 (2021).
10. Nastasi, C. et al. The effect of short-chain fatty acids on human monocyte-derived dendritic cells. *Sci. Rep.* **5**, 16148 (2015).
11. Furusawa, Y. et al. Commensal microbe-derived butyrate induces the differentiation of colonic regulatory T cells. *Nature* **504**, 446–450 (2013).
12. Sun, J. et al. Pancreatic beta-cells limit autoimmune diabetes via an immunoregulatory antimicrobial peptide expressed under the influence of the gut microbiota. *Immunity* **43**, 304–317 (2015).
13. Vandenbempt, V. et al. HAMSAB diet ameliorates dysfunctional signaling in pancreatic islets in autoimmune diabetes. *iScience* **27**, 108694 (2024).
14. Lamichhane, S. et al. Circulating metabolic signatures of rapid and slow progression to type 1 diabetes in islet autoantibody-positive children. *Front. Endocrinol.* **14**, 1211015 (2023).
15. Lamichhane, S. et al. Circulating metabolites in progression to islet autoimmunity and type 1 diabetes. *Diabetologia* **62**, 2287–2297 (2019).
16. Oresic, M. et al. Dysregulation of lipid and amino acid metabolism precedes islet autoimmunity in children who later progress to type 1 diabetes. *J. Exp. Med.* **205**, 2975–2984 (2008).
17. Winther, S. A. et al. Gut microbiota profile and selected plasma metabolites in type 1 diabetes without and with stratification by albuminuria. *Diabetologia* **63**, 2713–2724 (2020).
18. Jama, H. A. et al. Prebiotic intervention with HAMSAB in untreated essential hypertensive patients assessed in a phase II randomized trial. *Nat. Cardiovasc. Res.* **2**, 35–43 (2023).
19. Bell, K. J. et al. Metabolite-based dietary supplementation in human type 1 diabetes is associated with microbiota and immune modulation. *Microbiome* **10**, 9 (2022).
20. Gavin, P. G. et al. Metaproteomic sample preparation methods bias the recovery of host and microbial proteins according to taxa and cellular compartment. *J. Proteom.* **240**, 104219 (2021).
21. Lu, J. & Holmgren, A. The thioredoxin antioxidant system. *Free Radic. Biol. Med.* **66**, 75–87 (2014).
22. Zhou, P., Zhang, S., Wang, M. & Zhou, J. The induction mechanism of ferroptosis, necroptosis, and pyroptosis in inflammatory bowel disease, colorectal cancer, and intestinal injury. *Biomolecules* **13**, https://doi.org/10.3390/biom13050820 (2023).
23. Gasaly, N., Hermoso, M. A. & Gotteland, M. Butyrate and the fine-tuning of colonic homeostasis: implication for inflammatory bowel diseases. *Int. J. Mol. Sci.* **22**, https://doi.org/10.3390/ijms22063061 (2021).
24. Dong, S. et al. Effect of a humanized diet profile on colonization efficiency and gut microbial diversity in human flora-associated mice. *Front. Nutr.* **8**, 633738 (2021).
25. Rannug, A. How the AHR became important in intestinal homeostasis-a diurnal FICZ/AHR/CYP1A1 feedback controls both immunity and immunopathology. *Int. J. Mol. Sci.* **21**, https://doi.org/10.3390/ijms21165681 (2020).
26. Michaudel, C. et al. Rewiring the altered tryptophan metabolism as a novel therapeutic strategy in inflammatory bowel diseases. *Gut* **72**, 1296–1307 (2023).
27. Argelaguet, R. et al. Multi-Omics Factor Analysis—a framework for unsupervised integration of multi-omics data sets. *Mol. Syst. Biol.* **14**, e8124 (2018).
28. Park, S. W. et al. The protein disulfide isomerase AGR2 is essential for production of intestinal mucus. *Proc. Natl. Acad. Sci. USA* **106**, 6950–6955 (2009).
29. Othman, A., Sekheri, M. & Filep, J. G. Roles of neutrophil granule proteins in orchestrating inflammation and immunity. *FEBS J.* **289**, 3932–3953 (2022).
30. Phillipson, M. & Kubes, P. The healing power of neutrophils. *Trends Immunol.* **40**, 635–647 (2019).
31. Campbell, E. L. et al. Transmigrating neutrophils shape the mucosal microenvironment through localized oxygen depletion to influence the resolution of inflammation. *Immunity* **40**, 66–77 (2014).
32. Wang, R. X., Henen, M. A., Lee, J. S., Vogeli, B. & Colgan, S. P. Microbiota-derived butyrate is an endogenous HIF prolyl hydroxylase inhibitor. *Gut Microbes* **13**, 1938380 (2021).
33. Christoffersson, G. et al. VEGF-A recruits a proangiogenic MMP-9-delivering neutrophil subset that induces angiogenesis in transplanted hypoxic tissue. *Blood* **120**, 4653–4662 (2012).
34. Litvak, Y., Byndloss, M. X. & Baumler, A. J. Colonocyte metabolism shapes the gut microbiota. *Science* **362**, https://doi.org/10.1126/science.aat9076 (2018).
35. Marvel, D. & Gabrilovich, D. I. Myeloid-derived suppressor cells in the tumor microenvironment: expect the unexpected. *J. Clin. Investig.* **125**, 3356–3364 (2015).
36. Marti, I. L. A. A. & Reith, W. Arginine-dependent immune responses. *Cell Mol. Life Sci.* **78**, 5303–5324 (2021).
37. Barron, L. et al. Role of arginase 1 from myeloid cells in th2-dominated lung inflammation. *PLoS One* **8**, e61961 (2013).
38. Ji, L. et al. Slc6a8-mediated creatine uptake and accumulation reprogram macrophage polarization via regulating cytokine responses. *Immunity* **51**, 272–284.e277 (2019).
39. Nagaraj, S. et al. Altered recognition of antigen is a mechanism of CD8+ T cell tolerance in cancer. *Nat. Med* **13**, 828–835 (2007).
40. Lu, T. et al. Tumor-infiltrating myeloid cells induce tumor cell resistance to cytotoxic T cells in mice. *J. Clin. Investig.* **121**, 4015–4029 (2011).
41. Winter, S. E. et al. Host-derived nitrate boosts growth of *E. coli* in the inflamed gut. *Science* **339**, 708–711 (2013).
42. Hernandez, L. F., Buchwald, P. & Abdulreda, M. H. Effect of Arginase-1 inhibition on the incidence of autoimmune diabetes in NOD mice. *Curr. Res. Diabetes Obes. J.* **5** (2018).
43. Hesterberg, R. S., Cleveland, J. L. & Epling-Burnette, P. K. Role of polyamines in immune cell functions. *Med. Sci.* **6**, https://doi.org/10.3390/medsci6010022 (2018).
44. Kulkarni, A., Anderson, C. M., Mirmira, R. G. & Tersey, S. A. Role of polyamines and hypusine in beta cells and diabetes pathogenesis. *Metabolites* **12**, https://doi.org/10.3390/metabo12040344 (2022).
45. Karacay, C. et al. The effect of spermidine on autoimmunity and beta cell function in NOD mice. *Sci. Rep.* **12**, 4502 (2022).
46. Wagner, A. et al. Metabolic modeling of single Th17 cells reveals regulators of autoimmunity. *Cell* **184**, 4168–4185.e4121 (2021).
47. Sims, E. K. et al. Inhibition of polyamine biosynthesis preserves beta cell function in type 1 diabetes. *Cell Rep. Med.* **4**, 101261 (2023).
48. Pracht, K., Wittner, J., Kagerer, F., Jack, H. M. & Schuh, W. The intestine: a highly dynamic microenvironment for IgA plasma cells. *Front. Immunol.* **14**, 1114348 (2023).
49. Orabona, C. et al. Deficiency of immunoregulatory indoleamine 2,3-dioxygenase 1in juvenile diabetes. *JCI Insight* **3**, https://doi.org/10.1172/jci.insight.96244 (2018).
50. Li, S. Modulation of immunity by tryptophan microbial metabolites. *Front Nutr.* **10**, 1209613 (2023).
51. Pero, R. W., Lund, H. & Leanderson, T. Antioxidant metabolism induced by quinic acid. Increased urinary excretion of tryptophan and nicotinamide. *Phytother. Res.* **23**, 335–346 (2009).
52. Li, Y. et al. Tryptophan and the innate intestinal immunity: crosstalk between metabolites, host innate immune cells, and microbiota. *Eur. J. Immunol.* **52**, 856–868 (2022).
53. Booth, A. N., Robbins, D. J., Jones, F. T., Emerson, O. H. & Masri, M. S. Xanthurenic acid dehydroxylation by fecal microflora. *Proc. Soc. Exp. Biol. Med.* **120**, 546–548 (1965).

54. Kerkvliet, N. I. et al. Activation of aryl hydrocarbon receptor by TCDD prevents diabetes in NOD mice and increases Foxp3+ T cells in pancreatic lymph nodes. *Immunotherapy* **1**, 539–547 (2009).
55. Ehrlich, A. K. et al. Activation of the aryl hydrocarbon receptor by 10-Cl-BBQ prevents insulitis and effector T cell development independently of Foxp3+ regulatory T cells in nonobese diabetic mice. *J. Immunol.* **196**, 264–273 (2016).
56. Okada, M. et al. Islet-specific CD8(+) T cells gain effector function in the gut lymphoid tissues via bystander activation not molecular mimicry. *Immunol. Cell Biol.* **101**, 36–48 (2023).
57. Yap, Y. A. et al. An acetate-yielding diet imprints an immune and anti-microbial programme against enteric infection. *Clin. Transl. Immunol.* **10**, e1233 (2021).
58. Castro-Dopico, T. et al. Anti-commensal IgG drives intestinal inflammation and type 17 immunity in ulcerative colitis. *Immunity* **50**, 1099–1114.e1010 (2019).
59. Wu, W. et al. Microbiota metabolite short-chain fatty acid acetate promotes intestinal IgA response to microbiota which is mediated by GPR43. *Mucosal Immunol.* **10**, 946–956 (2017).
60. Isobe, J. et al. Commensal-bacteria-derived butyrate promotes the T-cell-independent IgA response in the colon. *Int. Immunol.* **32**, 243–258 (2020).
61. Round, J. L. & Palm, N. W. Causal effects of the microbiota on immune-mediated diseases. *Sci. Immunol.* **3**, https://doi.org/10.1126/sciimmunol.aao1603 (2018).
62. Buchanan, K. et al. An improved clinical model to predict stimulated C-peptide in children with recent-onset type 1 diabetes. *Pediatr. Diabetes* **20**, 166–171 (2019).
63. Gianetto, Q. G., Wieczorek, S., Couté, Y., & Burger, T. A peptide-level multiple imputation strategy accounting for the different natures of missing values in proteomics data. *bioRxiv*, https://doi.org/10.1101/2020.05.29.122770 (2020).
64. Peterson, A. L., Siddiqui, G., Sloan, E. K. & Creek, D. J. beta-Adrenoceptor regulation of metabolism in U937 derived macrophages. *Mol. Omics* **17**, 583–595 (2021).
65. Creek, D. J., Jankevics, A., Burgess, K. E., Breitling, R. & Barrett, M. P. IDEOM: an Excel interface for analysis of LC–MS-based metabolomics data. *Bioinformatics* **28**, 1048–1049 (2012).
66. Creek, D. J. et al. Toward global metabolomics analysis with hydrophilic interaction liquid chromatography-mass spectrometry: improved metabolite identification by retention time prediction. *Anal. Chem.* **83**, 8703–8710 (2011).
67. Han, J., Lin, K., Sequeira, C. & Borchers, C. H. An isotope-labeled chemical derivatization method for the quantitation of short-chain fatty acids in human feces by liquid chromatography-tandem mass spectrometry. *Anal. Chim. Acta* **854**, 86–94 (2015).
68. Liebisch, G. et al. Quantification of fecal short chain fatty acids by liquid chromatography tandem mass spectrometry-investigation of pre-analytic stability. *Biomolecules* **9**, https://doi.org/10.3390/biom9040121 (2019).
69. Adams, K. J. et al. Skyline for small molecules: a unifying software package for quantitative metabolomics. *J. Proteome Res.* **19**, 1447–1458 (2020).
70. Matsuki, T. et al. Development of 16S rRNA-gene-targeted group-specific primers for the detection and identification of predominant bacteria in human feces. *Appl. Environ. Microbiol.* **68**, 5445–5451 (2002).
71. Bolyen, E. et al. Reproducible, interactive, scalable and extensible microbiome data science using QIIME 2. *Nat. Biotechnol.* **37**, 852–857 (2019).
72. Bergot, A. S. et al. Regulatory T cells induced by single-peptide liposome immunotherapy suppress islet-specific T cell responses to multiple antigens and protect from autoimmune diabetes. *J. Immunol.* **204**, 1787–1797 (2020).
73. Rohart, F., Gautier, B., Singh, A. & Le Cao, K.-A. mixOmics: an R package for 'omics feature selection and multiple data integration. *PLoS Comput. Biol.* **13**, e1005752 (2017).
74. Oksanen, J. et al. vegan: Community Ecology Package_. R package version 2.6-2. (2022).
75. Hothorn, T., Bretz, F. & Westfall, P. Simultaneous inference in general parametric models. *Biometr. J.}* **50**, 346–363 (2008).
76. Ge, S. X., Jung, D. & Yao, R. ShinyGO: a graphical gene-set enrichment tool for animals and plants. *Bioinformatics* **36**, 2628–2629 (2020).
77. Yu, G., Xu, C., Zhang, D., Ju, F. & Ni, Y. MetOrigin: discriminating the origins of microbial metabolites for integrative analysis of the gut microbiome and metabolome. *iMeta* **1**, e10 (2022).
78. Young, M. D., Wakefield, M. J., Smyth, G. K. & Oshlack, A. Gene ontology analysis for RNA-seq: accounting for selection bias. *Genome Biol.* **11**, R14 (2010).
79. Perez-Riverol, Y. et al. The PRIDE database resources in 2022: a hub for mass spectrometry-based proteomics evidences. *Nucleic Acids Res.* **50**, D543–D552 (2022).

Acknowledgements

This work was supported by grants from the Juvenile Diabetes Research Foundation (JDRF) Australia (2-SRA-2019-703-M-B) and Children's Hospital Foundation (50316). EHW is supported by grants from the National Health and Medical Research Council (2002917, 2028813), JDRF International (3-SRA-2019-730-S-B) and JDRF Australia (201308399). ENG is a Research Associate of the FNRS, Belgium. This research was carried out at the Translational Research Institute, Woolloongabba, QLD 4102, Australia. The Translational Research Institute is supported by a grant from the Australian Government. We would like to thank Yu Anne Yap and the staff in the Translational Research Institute Gnotobiotic animal and the Translational Research Institute Proteomics facility for technical support. We thank the NIH Tetramer Core Facility for providing MHC-I tetramers. Figures 1A, 2F, 4A, 5E and 5F were created in Biorender.

Author contributions

B.T. contributed to study design, performed proteomics, data analysis, curation and visualization, statistical analysis, and co-wrote the manuscript. J.D. performed formal analysis, data curation, bioinformatics and statistics, and data visualization. K.S., T.G., and V.Z. performed animal experiments, collected data, and performed analysis. D.A., D.C., C.K.B. and T.S. developed methodology, performed metabolomics analysis and reviewed the manuscript. E.D. developed methodology and supervised gnotobiotic animal experiments. MM developed methodology, contributed to funding acquisition and reviewed the manuscript. M.M.H. developed methodology, provided resources, supervised T.S. and edited the manuscript. R.G. developed methodology, performed investigations, data analysis and edited the manuscript. J.B.: developed methodology, provided resources, supervised R.G. and edited the manuscript. D.L. performed proteomic analysis. E.G., S.S. and K.B. co-designed the clinical study, acquired funding and K.B. carried out the clinical study and clinical data analysis. C.W.C. performed data analysis and statistics, supervised J.D. and edited the manuscript. E.M. conceptualized and co-designed the study, provided resources, supervised J.D., acquired funding and co-wrote the manuscript. E.H.W. conceptualized and co-designed the study, provided resources, supervised B.T., K.S., T.G. and V.Z., acquired funding and co-wrote the manuscript.

Competing interests

E.M. is an inventor on a patent WO2018027274A1 submitted by Monash University that covers methods and compositions for metabolites for the treatment and prevention of autoimmune disease related to this paper, and is the founder of ImmunoBiota Therapeutics Pty Ltd. All other authors declare no competing interests.

Additional information

Supplementary information The online version contains supplementary material available at https://doi.org/10.1038/s41467-025-58319-y.

Correspondence and requests for materials should be addressed to Eliana Mariño or Emma E. Hamilton-Williams.

Peer review information *Nature Communications* thanks the anonymous reviewers for their contribution to the peer review of this work. A peer review file is available.

[1]Frazer Institute, The University of Queensland, Brisbane, QLD, Australia. [2]Department of Medical Microbiology, Faculty of Medicine, University of Malaya, Kuala Lumpur, Malaysia. [3]Monash Institute of Pharmaceutical Sciences, Monash University, Melbourne, VIC, Australia. [4]Monash Proteomics and Metabolomics Platform, Monash University, MelbourneVIC, Australia. [5]Translational Research Institute, Brisbane, QLD, Australia. [6]Mater Research Institute—The University of Queensland, Brisbane, QLD, Australia. [7]QIMR Berghofer Medical Research Institute, Brisbane, QLD, Australia. [8]Department of Gastroenterology and Hepatology, Princess Alexandra Hospital, Brisbane, QLD, Australia. [9]Signal Transduction and Metabolism Laboratory, Université libre de Bruxelles, Brussels, Belgium. [10]Charles Perkins Centre, University of Sydney, Sydney, NSW, Australia. [11]Department of Medicine, Kolling Institute, University of Sydney, Sydney, NSW, Australia. [12]Department of Biochemistry, Biomedicine Discovery Institute, Monash University, Melbourne, VIC, Australia. [13]Monash University Microbiome Research Centre, School of Pharmacy, Monash University Malaysia, Selangor, Malaysia. [14]ImmunoBiota Therapeutics Pty Ltd, Melbourne, VIC, Australia. [15]These authors contributed equally: Eliana Mariño, Emma E. Hamilton-Williams. ✉e-mail: eliana.marino@monash.edu; e.hamiltonwilliams@uq.edu.au